EUROPEAN ORGANIZATION FOR NUCLEAR RESEARCH

CERN-EP-2024-228
06 September 2024

Exploring nuclear structure with multiparticle azimuthal correlations at the LHC

ALICE Collaboration*

Abstract

Understanding nuclear structure provides essential insights into the properties of atomic nuclei. In this paper, details of the nuclear structure of ^{129}Xe, such as the quadrupole deformation and the nuclear diffuseness, are studied by extensive measurements of anisotropic-flow-related observables in Xe–Xe collisions at a center-of-mass energy per nucleon pair $\sqrt{s_{\mathrm{NN}}} = 5.44$ TeV with the ALICE detector at the LHC. The results are compared with those from Pb–Pb collisions at $\sqrt{s_{\mathrm{NN}}} = 5.02$ TeV for a baseline, given that the ^{208}Pb nucleus is not deformed. Furthermore, comprehensive comparisons are performed with a state-of-the-art hybrid model using IP-Glasma+MUSIC+UrQMD. It is found that among various IP-Glasma+MUSIC+UrQMD calculations with different values of nuclear parameters, the one using a nuclear diffuseness parameter of $a_0 = 0.492$ and a nuclear quadrupole deformation parameter of $\beta_2 = 0.207$ provides a better description of the presented flow measurements. These studies represent an important step towards a thorough exploration of the imaging power of nuclear collisions at ultrarelativistic energy and the search for the imprint of nuclear structure on various flow observables in heavy-ion collisions at the LHC. The findings demonstrate the potential of nuclear structure studies at the TeV energy scale and highlight that the LHC experiments can complement existing low-energy experiments on nuclear structure studies.

*See Appendix A for the list of collaboration members

1 Introduction

Studies of nuclear structure contribute to the understanding of nuclide properties. Over the past few decades, low-energy nuclear physics has achieved impressive progress [1–14]. These advancements have led to the accurate determination of nuclear charge radii for light and medium mass nuclei [6–11]. Additionally, the properties of light nuclei with a mass number $A \leq 50$ have been elucidated [6–8, 12–14], particularly with the advent of modern *ab-initio* methods addressing the nuclear many-body problem [1–5]. Nevertheless, accurately determining the neutron skin thickness and the shape of nuclei remains a challenging task due to their intricate nature [15–20]. Furthermore, applying *ab-initio* methods to heavy nuclei is challenging due to the computational complexity that arises from the need to accurately model the strong interactions among an increasing number of nucleons [21]. Recent studies in high-energy heavy-ion collisions at the Relativistic Heavy-Ion Collider (RHIC) [22–26] and the Large Hadron Collider (LHC) [27–31] have demonstrated that nuclear collisions at ultrarelativistic energies could serve as new avenues for nuclear structure studies. These studies successfully probed the nuclear shape from light to heavy nuclei [24–26, 32–37] and the neutron skin of ^{208}Pb, ^{96}Zr, and ^{96}Ru [18, 38]. Among these experimental approaches, anisotropic flow phenomena have been found to carry the imaging power of the nuclear structures at relativistic energies [24, 32, 39–45]. Anisotropic flow, which quantifies the anisotropic azimuthal distribution of the momenta of the produced particles, reflects the initial geometry and fluctuations of the overlapping region and probes the shape (or structure) of the colliding nuclei [46–51]. The anisotropic flow is characterized by the Fourier expansion of the azimuthal distribution of produced particles [52]

$$\frac{dN}{d\varphi} \propto 1 + 2\sum_{n=1}^{\infty} v_n \cos[n(\varphi - \Psi_n)], \tag{1}$$

where φ is the azimuthal angle of particle momentum and Ψ_n is the n^{th}-order symmetry plane. The coefficients v_n are called flow coefficients and can be calculated as

$$v_n = \langle \cos[n(\varphi - \Psi_n)] \rangle \,. \tag{2}$$

Here, the brackets $\langle\rangle$ denote an average over all particles in one event. With v_n and Ψ_n, the n$^{\text{th}}$ order (complex) anisotropic flow V_n are defined as

$$V_n \equiv v_n \mathrm{e}^{in\Psi_n}. \tag{3}$$

A comprehensive exploration of the anisotropic flow phenomena, encompassing systematic measurements of v_n [22, 27, 31, 53–58], event-by-event flow fluctuations [59–64], and correlations between various flow coefficients [65–70], has been previously reported. These observables effectively capture a snapshot of the initial geometry of the collision and, by extension, offer a glimpse into the structure of the colliding nuclei.

For the initial state of heavy-ion collisions, the nuclear density profile $\rho(r,\theta,\phi)$ of the colliding nuclei can be described by the Woods–Saxon distribution [41, 71]

$$\rho(r,\theta,\phi) = \frac{\rho_0}{1 + e^{[r-R(\theta,\phi)]/a_0}}, \tag{4}$$

where r, θ, and ϕ define the position of a nucleon presented in spherical coordinates, of which the origin is the center of the nucleus. The constant ρ_0 ensures that the integral of the distribution corresponds to the number of nucleons in the nucleus. The a_0 parameter represents the nuclear diffuseness. The $R(\theta,\phi) = R_0(1+\beta_2[\cos\gamma Y_{2,0} + \sin\gamma Y_{2,2}])$ term models the nuclear surface expanded in terms of spherical harmonics $Y_{n,m}$, keeping terms up to $n = 2$ that are the most relevant in the structure of ^{129}Xe [28, 35, 40]. Notably, $Y_{2,-2}$, $Y_{2,-1}$, and $Y_{2,1}$ are utilized to establish the intrinsic frame, which renders $Y_{2,0}$ and $Y_{2,2}$ as the only pertinent degrees of freedom. In $R(\theta,\phi)$, R_0 denotes the nuclear radius, and β_2 is the quadrupole deformation parameter. In low-energy nuclear experiments, β_2 for even-A isotopes of Xe can be measured using the electric quadrupole transition probability B(E2)↑ from the ground 0^+ to the first-excited 2^+ state [72, 73]. By interpolating the values between ^{128}Xe and ^{130}Xe, β_2 for ^{129}Xe was estimated to be 0.18 ± 0.02 [28]. Finally, the triaxial parameter γ reflects the inequality of the axes of the spheroid.

This Letter presents systematic measurements of various flow observables using charged particles from Xe–Xe collisions at a center-of-mass energy per nucleon pair $\sqrt{s_{\rm NN}} = 5.44$ TeV recorded by the ALICE detector. In addition, the corresponding measurements from Pb–Pb collisions at $\sqrt{s_{\rm NN}} = 5.02$ TeV, which provide a baseline because of the spherical shape of ^{208}Pb [72], are shown. Observables used in this study, including flow coefficients, flow fluctuations, nonlinear flow modes, and correlations between flow coefficients, are introduced in Sec. 2. Section 3 presents the experimental setup and the evaluation of systematical uncertainties. The results are discussed in Sec. 4, followed by the summary in Sec. 5.

2 Observables and analysis method

Flow coefficients v_n are usually measured by using two and four-particle cumulants [74–77]

$$\begin{aligned} v_n\{2\} &\equiv \sqrt{c_n\{2\}}, \\ v_n\{4\} &\equiv \sqrt[4]{-c_n\{4\}}, \end{aligned} \tag{5}$$

where $c_n\{2\}$ and $c_n\{4\}$ are the two and four-particle cumulants, respectively. It is known that $v_n\{2\}$ and $v_n\{4\}$ carry opposite contributions from flow fluctuations to the cumulant estimates [78]. When non-flow effects, which are the azimuthal angle correlations not associated with the symmetry plane, are small, the flow coefficients can be split into mean flow and flow fluctuation according to

$$\begin{aligned} v_n\{2\}^2 &\approx \langle v_n \rangle^2 + \sigma_{v_n}^2, \\ v_n\{4\}^2 &\approx \langle v_n \rangle^2 - \sigma_{v_n}^2. \end{aligned} \tag{6}$$

Here σ_{v_n} is the standard deviation of the v_n distribution, known as event-by-event fluctuation of v_n, and $\langle v_n \rangle$ is the mean value of the v_n distribution.

For $n = 2$ and $n = 3$, v_n coefficients for central and midcentral collisions are linearly correlated with the initial anisotropy coefficients ε_n [79, 80], where ε_n is determined from the initial energy density profile [81]

$$\varepsilon_n e^{in\Phi_n} = -\frac{\langle r^n e^{in\phi} \rangle}{\langle r^n \rangle} \; (n > 1), \tag{7}$$

where $\langle\rangle$ represents an average among the transverse positions (r, ϕ) of all participating nucleons, with ϕ representing the azimuthal angle and r characterizing the radial distance from the origin of the system. The Φ_n angle defines the symmetry plane of participant nucleons in the initial conditions. Recent studies have shown that nuclear quadrupole deformation strongly affects the initial eccentricity, particularly in the most central collisions [24, 32, 41]. Therefore, the final state v_n is expected to be an ideal tool to probe the deformations.

The high order flow coefficients v_n $(n > 3)$ receive contributions not only from the linear response to the initial ε_n but also from the nonlinear response originated from lower order ε_2 and/or ε_3 [82–84]. For example, the 4$^{\rm th}$ order (complex) anisotropic flow V_4 can be decomposed into linear ($V_4^{\rm L}$) and nonlinear ($V_4^{\rm NL}$) components according to

$$V_4 = V_4^{\rm L} + V_4^{\rm NL}, \tag{8}$$

whose magnitudes are denoted by v_4^{L} and $v_{4,22}$, respectively. The subscript of $v_{4,22}$ represents the part of v_4 coming from ε_2^2 [82–84]. In Eq. (8) V_4^{L} and V_4^{NL} are considered to be uncorrelated and $v_{4,22}$ can be measured via a projection of V_4 onto the direction of V_2 [66, 84]

$$v_{4,22} = \frac{\Re\langle V_4 (V_2^*)^2 \rangle}{\sqrt{\langle |V_2|^4 \rangle}}. \tag{9}$$

The magnitude of the linear component can be easily derived as $v_4^{\mathrm{L}} = \sqrt{v_4^2\{2\} - v_{4,22}^2}$.

Furthermore, the correlation between the symmetry planes Ψ_4 and Ψ_2 can be probed via the nonlinear flow correlation $\rho_{4,22}$ proposed in Ref. [84]. It is defined by the ratio of $v_{4,22}$ and $v_4\{2\}$

$$\rho_{4,22} = \frac{v_{4,22}}{v_4\{2\}} \approx \langle \cos(4\Psi_4 - 4\Psi_2) \rangle. \tag{10}$$

In addition, the nonlinear component V_4^{NL} can be further decomposed as

$$\begin{aligned} V_4^{\mathrm{NL}} &\approx \chi_{4,22} (V_2)^2, \\ \chi_{4,22} &= \frac{v_{4,22}}{\sqrt{\langle |V_2|^4 \rangle}} = \frac{\Re\langle V_4 (V_2^*)^2 \rangle}{\langle |V_2|^4 \rangle}, \end{aligned} \tag{11}$$

where $\chi_{4,22}$ is called the nonlinear flow-mode coefficient. It represents the strength of nonlinear response to V_4 and is independent of ε_2. Recent studies with both transport and hydrodynamic model calculations have shown that nonlinear flow mode observables such as $v_{4,22}$, $\rho_{4,22}$, and $\chi_{4,22}$, owing to their different sensitivities to different stages of heavy-ion collisions [74, 82, 85–88], bring distinction power to the study of deformation of the colliding nuclei [33, 42, 44].

Previous studies also showed that the correlations between different flow coefficients are sensitive to the initial conditions as well as the dynamic evolution of the created systems [65, 69, 74, 89], which can be quantified by the normalized symmetric cumulants (NSC) [74] according to

$$\mathrm{NSC}(m,n) = \frac{\langle v_m^2 v_n^2 \rangle - \langle v_m^2 \rangle \langle v_n^2 \rangle}{\langle v_m^2 \rangle \langle v_n^2 \rangle}. \tag{12}$$

As also in the previous cases, the bracket $\langle\rangle$ denotes an average over all events. The $\mathrm{NSC}(m,n)$ results will be positive, zero, or negative if v_n^2 and v_m^2 are correlated, uncorrelated, or anticorrelated, respectively.

All the observables mentioned above are based on two- and multiparticle correlations, which can be obtained using the *Generic Framework* [74, 77, 90] for the flow studies. To suppress non-flow contributions, a pseudorapidity gap $|\Delta\eta| > 1.0$ was applied in the two-particle correlations in the second harmonic. For high order ($n \geq 3$) correlations, a looser pseudorapidity gap of $|\Delta\eta| > 0.8$ was applied to preserve more particles for the analysis, considering the limited size of the Xe–Xe data sample. For the multiparticle correlations, which are less sensitive to non-flow contaminations, $|\Delta\eta| > 0.8$ was also applied, except for $v_2\{4\}$, where the pseudorapidity gap is unnecessary as their potential non-flow effects are negligible [77, 91].

Except $v_2\{2\}$, $v_3\{2\}$, $v_4\{2\}$, and $v_2\{4\}$, which are taken from Ref. [27], the other observables are measured for the first time in Xe–Xe collisions. For Pb–Pb collisions, measurements of most observables were significantly improved after using the entire Run 2 data compared with previous measurements based only on the 2015 data sample [54, 59, 68, 69].

3 Analysis Details

The data sample analyzed in this study was recorded by the ALICE detector [92–95] during the Xe–Xe run at $\sqrt{s_{\mathrm{NN}}} = 5.44$ TeV in 2017 and Pb–Pb runs at $\sqrt{s_{\mathrm{NN}}} = 5.02$ TeV in 2015 and 2018 at the

LHC. Minimum bias events were triggered by the coincidence of two scintillator counter arrays, V0A and V0C [92, 96], covering the pseudorapidity intervals $2.8 < \eta < 5.1$ and $-3.7 < \eta < -1.7$, respectively. Additional Pb–Pb events in the 0–10% and 30–50% centrality classes were recorded in 2018, using central and semicentral triggers, respectively, to maximize the integrated luminosity for central and semiperipheral collisions. Pile-up events, where multiple collisions are included in one single event, were rejected using the timing information from the V0 detectors and selections on the correlation of the multiplicity measured by the Inner Tracking System (ITS) [92, 97] and the the Time Projection Chamber (TPC) [92, 98]. Charged particles are reconstructed in the central pseudorapidity region from their hits in the ITS, which is composed of six layers of silicon detectors surrounding the beam vacuum tube, and the TPC. The track reconstruction in the ITS and the TPC provided the information on the primary vertex. The position of the primary vertex along the beam direction, V_z, was required to be within $\pm$ 10 cm from the center of the detector. The analysis was performed as a function of collision centrality, determined using the information from the V0 detectors [28, 99] and expressed as percentiles of the total inelastic Xe–Xe or Pb–Pb cross sections. The whole centrality range considered in this analysis was 0–60%, where 0% corresponds to the most central collisions. After the event selection, about 0.8 million Xe–Xe events and 163 million Pb–Pb events were analyzed in this work.

Charged-particle tracks in the pseudorapidity region $|\eta| < 0.8$ and transverse momentum region $0.2 < p_{\mathrm{T}} < 3.0$ GeV/c were selected for the analysis. The track quality was ensured by requiring at least 70 TPC space points out of a maximum of 159 with an average χ^2 per degree of freedom of the track fit lower than 2.5. The distance of the closest approach (DCA) to the primary vertex in the beam direction, DCA$_z$, was required to be less than 2 cm. In addition, the DCA in the transverse plane was required to be $\mathrm{DCA}_{xy} < 0.0105 + 0.0350 p_{\mathrm{T}}^{-1.1}$ cm, with p_{T} measured in GeV/c, which gives a p_{T}-dependent selection on DCA$_{xy}$ with thresholds at 0.22 cm at 0.2 GeV/c and 0.02 cm at 3.0 GeV/c. A p_{T}-dependent weight obtained from simulations performed with the HIJING event generator [100, 101] combined with the GEANT3 transport code [102] was applied to correct for the track reconstruction efficiency. The track reconstruction efficiency ranges from 62% to 80% for $p_{\mathrm{T}} < 1.0$ GeV/c, and drops slightly for higher p_{T} reaching a roughly constant value of about 76%. In addition, φ distributions of the reconstructed tracks were utilized for extracting a non-uniform acceptance correction.

The sources of systematic uncertainty have been investigated by varying the criteria for selecting events and tracks. For event selections, the requirement for primary vertex position from the center of the detector V_z was varied to ± 5, ± 7, and ± 9 cm, respectively. In addition, the centrality estimation was alternatively determined by using the number of hits in the second-most internal layer of the ITS. In general, these sources yield uncertainties below 1%; except the uncertainties associated with centrality estimation for $v_{4,22}$, $\rho_{4,22}$, and $\chi_{4,22}$ which are above 1%. Furthermore, the systematic effect from pile-up events was studied by varying the selections on the correlations between multiplicities from the ITS and the TPC was found to be negligible.

Similarly, for the track selections, the minimum number of TPC space points was varied to 80, 90, and 100. The requirement for DCA$_{xy}$ was changed to $\mathrm{DCA}_{xy} < 0.0090 + 0.0300 p_{\mathrm{T}}^{-1.1}$ cm, with p_{T} measured in GeV/c, while DCA$_z$ was required to be within 1.0 or 0.5 cm. These sources typically result in uncertainties of less than 1%. Finally, the systematic uncertainties that were statistically significant according to the recommendation in Ref. [103] were added in quadrature to obtain the total systematic uncertainty. The total systematic uncertainties are typically less than 2% in the 0–60% centrality range, and they are denoted as gray boxes in the figures in Sec. 4.

4 Results

Figure 1 presents the measurements of $v_2\{m\}(m = 2, 4)$ in Xe–Xe and Pb–Pb collisions as a function of centrality. In the upper panels, $v_2\{2, |\Delta\eta| > 1.0\}$ and $v_2\{4\}$ are shown. They increase from central to pe-

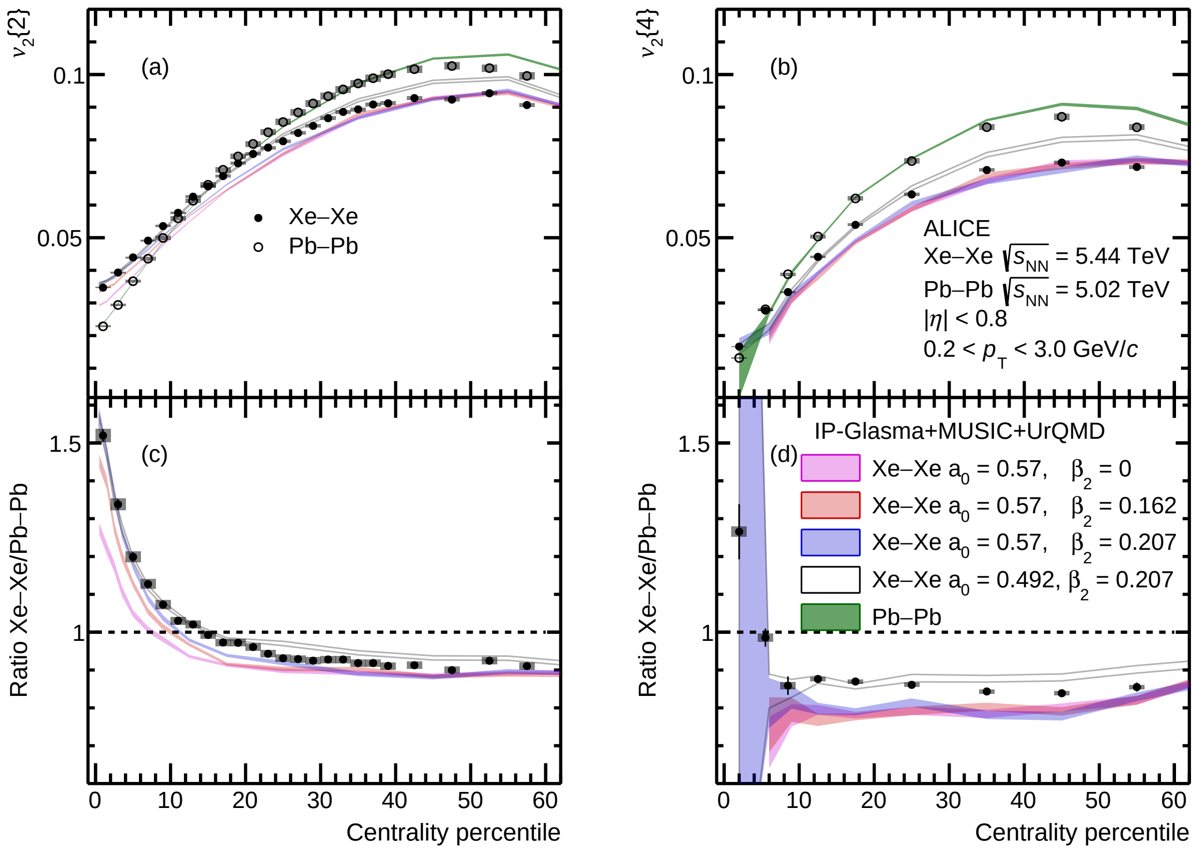

Figure 1: Panels (a) and (b): Charged particle $v_2\{2, |\Delta\eta| > 1.0\}$ (left) and $v_2\{4\}$ (right) as a function of centrality in Xe–Xe and Pb–Pb collisions at $\sqrt{s_{\rm NN}}$ = 5.44 TeV and $\sqrt{s_{\rm NN}}$ = 5.02 TeV, respectively. Panels (c) and (d): Ratio between Xe–Xe and Pb–Pb $v_2\{2, |\Delta\eta| > 1.0\}$ (left) and $v_2\{4\}$ (right). Statistical and systematical uncertainties are shown as vertical lines and gray boxes, respectively. The measurements are compared with IP-Glasma+MUSIC+UrQMD calculations [104, 105] to constrain the β_2 and a_0 parameters of ^{129}Xe nuclei.

ripheral Xe–Xe and Pb–Pb collisions. The comparisons between Xe–Xe and Pb–Pb results are quantified as ratios in the bottom panels. Considering the similar dynamic evolution of the created matter in Pb–Pb and Xe–Xe collisions, the ratios of flow observables should largely cancel the final state effects and thus mainly reflect the information on the initial conditions, including the nuclear structure. This has been validated in recent hydrodynamic and transport model calculations [44, 106]. Both $v_2\{2, |\Delta\eta| > 1.0\}$ and $v_2\{4\}$ ratios decrease steeply with increasing centrality percentile in central collisions and then level off for midcentral collisions. The $v_2\{2, |\Delta\eta| > 1.0\}$ ratio starts at approximately 1.5 in the most central collisions and is larger than unity in the centrality range 0–15%, whereas the $v_2\{4\}$ ratio starts at approximately 1.3 and is above unity only in the 5% most central collisions. In a central collision, the fluctuations of the overlap region play a dominant role, and smaller system size (Xe–Xe collisions) generates stronger fluctuations [107], which cause both ratios to be larger than unity. In addition, the deformation of ^{129}Xe nuclei further enhances ε_2 in ultracentral collisions of 0–5% centrality; this effect will be discussed in detail later. In midcentral collisions, $v_2\{2, |\Delta\eta| > 1.0\}$ and $v_2\{4\}$ ratios remain at approximately 0.9 and 0.85, respectively. The ratios are below unity due to viscous effects during the medium expansion [27, 108, 109].

The measurements are compared with calculations using the sequential combination of the impact-parameter Glasma (IP-Glasma) initial conditions, MUSIC relativistic hydrodynamic model, and the ultrarelativistic quantum molecular dynamics (UrQMD) model for hadronic rescatterings. This hybrid model is denoted as IP-Glasma+MUSIC+UrQMD [104, 105]. These calculations are presented as bands of different colors in Figs. 1 to 6, where the bandwidths denote the uncertainties of calculations. To investigate the impact of nuclear structure, different initial conditions were used for Xe–Xe calculations, varying the β_2 quadrupole deformation and the a_0 nuclear diffuseness. The values of β_2 and a_0 were adopted based on existing predictions. Specifically, $a_0 = 0.492$ and $\beta_2 = 0.207$ are taken from Ref. [35], $\beta_2 = 0.162$ is from Ref. [110], and $a_0 = 0.57$ is used in Ref. [28]. Notably, the setting of $\beta_2 = 0$ represents a special scenario of a spherical ^{129}Xe nucleus. In Fig. 1, the IP-Glasma+MUSIC+UrQMD calculations in Pb–Pb collisions (green shadows) align well with the measurements of $v_2\{2,|\Delta\eta| > 1.0\}$ and $v_2\{4\}$ up to a centrality of 40%. However, beyond 40% centrality, the calculated values exceed the measurements. For Xe–Xe, in the 0–15% centrality range, the calculations with $a_0 = 0.57, \beta_2 = 0.207$ (blue shadows) and $a_0 = 0.492, \beta_2 = 0.207$ (hollow bands) match the measurements of $v_2\{2,|\Delta\eta| > 1.0\}$ better, while they underestimate $v_2\{4\}$ in 5–10% centrality. Then for the 15–25% centrality range, the measurements of $v_2\{2,|\Delta\eta| > 1.0\}$ and $v_2\{4\}$ are better described by the calculations when the parameters are set to $a_0 = 0.492, \beta_2 = 0.207$ (hollow bands). Furthermore, in the 35–60% centrality range, the calculations with $a_0 = 0.57, \beta_2 = 0.207$ (blue shadows), as well as $a_0 = 0.57, \beta_2 = 0.162$ (red shadows) and $a_0 = 0.57, \beta_2 = 0$ (pink shadows) provide better descriptions for the measurements of both $v_2\{2,|\Delta\eta| > 1.0\}$ and $v_2\{4\}$. Notably in the 0–10% centrality range in Fig. 1(c), the calculations for $v_2\{2,|\Delta\eta| > 1.0\}$ with $a_0 = 0.57, \beta_2 = 0.162$ and $a_0 = 0.57, \beta_2 = 0$ are approximately 5% and 20% lower, respectively, than the measured ratios of Xe–Xe and Pb–Pb results. This discrepancy highlights the contributions from the quadrupole deformation of ^{129}Xe [32, 33, 41, 42, 44]. In this centrality range, the initial shape of the overlapping region is primarily determined by the shape of the colliding nuclei; thus, the deformed nuclei enhance the initial eccentricity ε_2 of the overlapping region, consequently leading to larger v_2.

As introduced in Eq. (6), $v_2\{2\}$ and $v_2\{4\}$ receive contributions from both $\langle v_2 \rangle$ and its event-by-event fluctuations σ_{v_2}. Consequently, mean flow and flow fluctuations can be measured separately using the combination of $v_2\{2\}$ and $v_2\{4\}$. Figure 2 presents the centrality dependence of $\langle v_2 \rangle$ and σ_{v_2} in Xe–Xe and Pb–Pb collisions. In panel (a), $\langle v_2 \rangle$ increases from central to peripheral collisions for both Xe–Xe and Pb–Pb collisions. The ratio between Xe–Xe and Pb–Pb $\langle v_2 \rangle$ in panel (c) exceeds unity in 0–10% centrality, then decreasing to approximately 0.9 in the midcentral collisions. Overall, σ_{v_2} in Xe–Xe is larger than in Pb–Pb in the whole 0–60% centrality range, attributable to the smaller system size of Xe–Xe collisions [107]. The ratio between Xe–Xe and Pb–Pb σ_{v_2} in panel (d) starts at approximately 1.5 in the most central collisions and steadily decreases with increasing centrality percentile, converging to unity at 60% centrality. For $\langle v_2 \rangle$ in Fig. 2(a) and (c), the IP-Glasma+MUSIC+UrQMD calculations with $\beta_2 = 0.207$ describe the measurements in 0–10% centrality. Due to the extensive statistical samples required, other calculations are only available for centralities above 5%, which notably underestimate the measured $\langle v_2 \rangle$ for the 0–20% centrality range. For σ_{v_2} shown in Fig. 2(b) and (d), most calculations describe the measurements within the presented centrality range, except for the one with $a_0 = 0.57$ and $\beta_2 = 0$, which falls below the measurement in 0–20% centrality. A weaker elliptic flow fluctuation σ_{v_2} is seen in central Xe–Xe collisions when a spherical nuclear structure of ^{129}Xe is used in the model calculations. In more peripheral collisions, the IP-Glasma+MUSIC+UrQMD calculation with $a_0 = 0.492$ underestimates the measured σ_{v_2}, while those with $a_0 = 0.57$ agree with the measurement. For centrality above 20%, the calculations for σ_{v_2} with different a_0 and β_2 are compatible with each other within uncertainties, suggesting that σ_{v_2} might not depend on the nuclear diffuseness and deformation for non-central collisions.

In addition to the study of elliptic flow v_2 and its event-by-event fluctuations, the triangular flow $v_3\{2\}$ and quadrangular flow $v_4\{2\}$, which provide more precise constraints on the initial conditions [81, 111], are also examined as a function of centrality in Fig. 3. In the upper panels, $v_3\{2,|\Delta\eta| > 0.8\}$ is notably larger in Xe–Xe than in Pb–Pb within the 0–35% centrality range, while the $v_3\{2,|\Delta\eta| > 0.8\}$ measurements in Xe–Xe are smaller for more peripheral collisions. The $v_4\{2,|\Delta\eta| > 0.8\}$ results are compatible

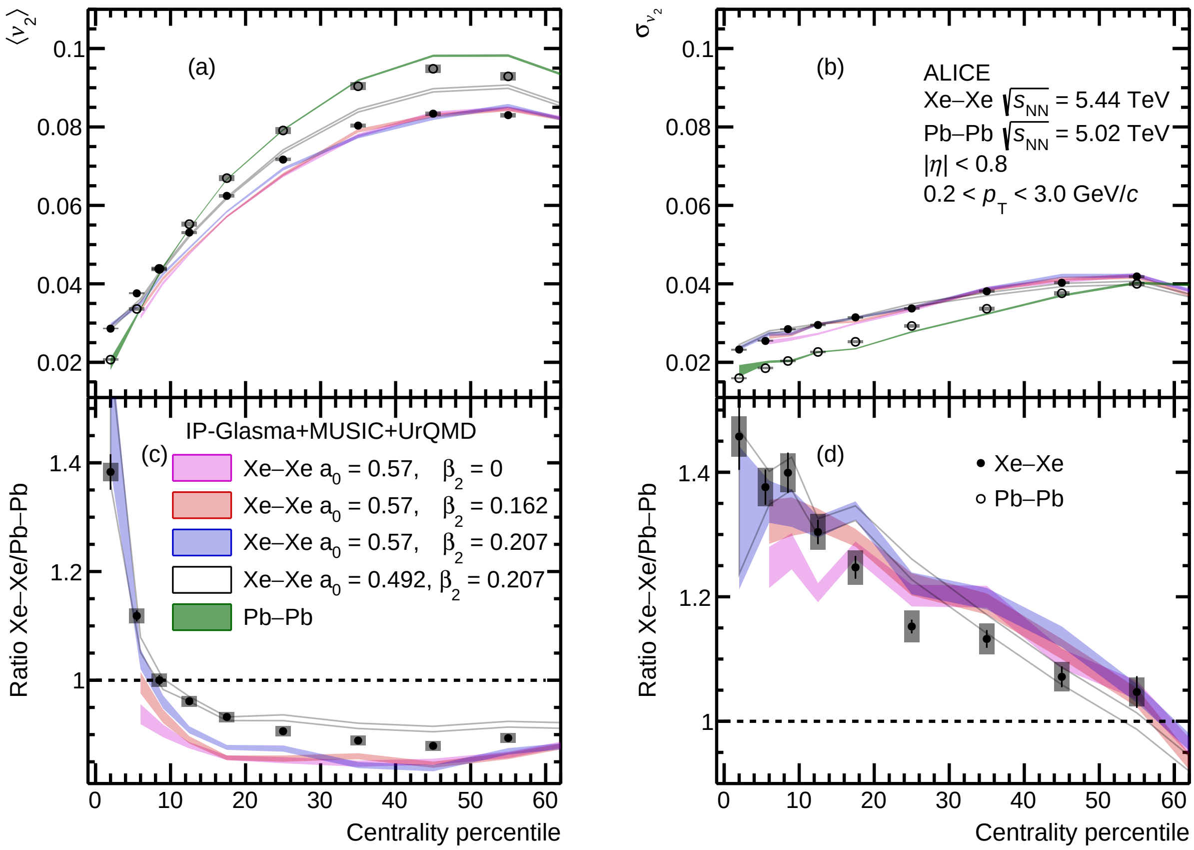

Figure 2: Panels (a) and (b): Charged particle $\langle v_2 \rangle$ (left) and σ_{v_2} (right) as a function of centrality in Xe–Xe and Pb–Pb collisions at $\sqrt{s_{\rm NN}} = 5.44$ TeV and $\sqrt{s_{\rm NN}} = 5.02$ TeV, respectively. Panels (c) and (d): Ratio between Xe–Xe and Pb–Pb $\langle v_2 \rangle$ (left) and σ_{v_2} (right). Statistical and systematical uncertainties are shown as vertical lines and gray boxes, respectively. The measurements are compared with IP-Glasma+MUSIC+UrQMD calculations [104, 105] to constrain the β_2 and a_0 parameters of ^{129}Xe nuclei.

within uncertainties for both Xe–Xe and Pb–Pb collisions up to 30% centrality, after which Xe–Xe results are smaller than those in Pb–Pb collisions. In the lower panels, accordingly, the ratios between Xe–Xe and Pb–Pb $v_3\{2,|\Delta\eta|>0.8\}$ and $v_4\{2,|\Delta\eta|>0.8\}$ decrease steadily with increasing centrality. The IP-Glasma+MUSIC+UrQMD calculations are lower than the $v_3\{2,|\Delta\eta|>0.8\}$ measurements in Pb–Pb collisions up to 40% centrality, beyond which the calculations overestimate the measurements. A similar pattern is observed for Xe–Xe collisions, where the calculations are roughly compatible with the $v_3\{2,|\Delta\eta|>0.8\}$ measurements in central collision and exceed the measured values for centrality above 20%. Meanwhile, no difference is found among the $v_3\{2,|\Delta\eta|>0.8\}$ calculations with different β_2 values. This is consistent with the expectation that $v_3\{2\}$, which is primarily driven by the linear response to the initial triangularity ε_3 [79, 80], may be sensitive to octupole deformation β_3 but not to quadrupole deformation β_2. This has also been confirmed in the previous AMPT model studies [44]. Furthermore, for the Xe–Xe/Pb–Pb ratios in Fig. 3, the calculations qualitatively capture the general trend of the centrality dependence of the measured $v_3\{2,|\Delta\eta|>0.8\}$ and $v_4\{2,|\Delta\eta|>0.8\}$. However, all calculations for $v_3\{2,|\Delta\eta|>0.8\}$ ratio are higher than the measurements in 10–40% centrality. A distinction is observed between calculations from $a_0 = 0.57$ and $a_0 = 0.492$ in the 10–40% centrality range; the latter exhibits a slightly better agreement with the measurement. Concurrently, the calculations appear to overestimate the $v_4\{2,|\Delta\eta|>0.8\}$ ratio in central collisions, despite large uncertainties. A difference between the calculations of $v_4\{2,|\Delta\eta|>0.8\}$ with $a_0 = 0.57$ and $a_0 = 0.492$ is also noted in more peripheral collisions,

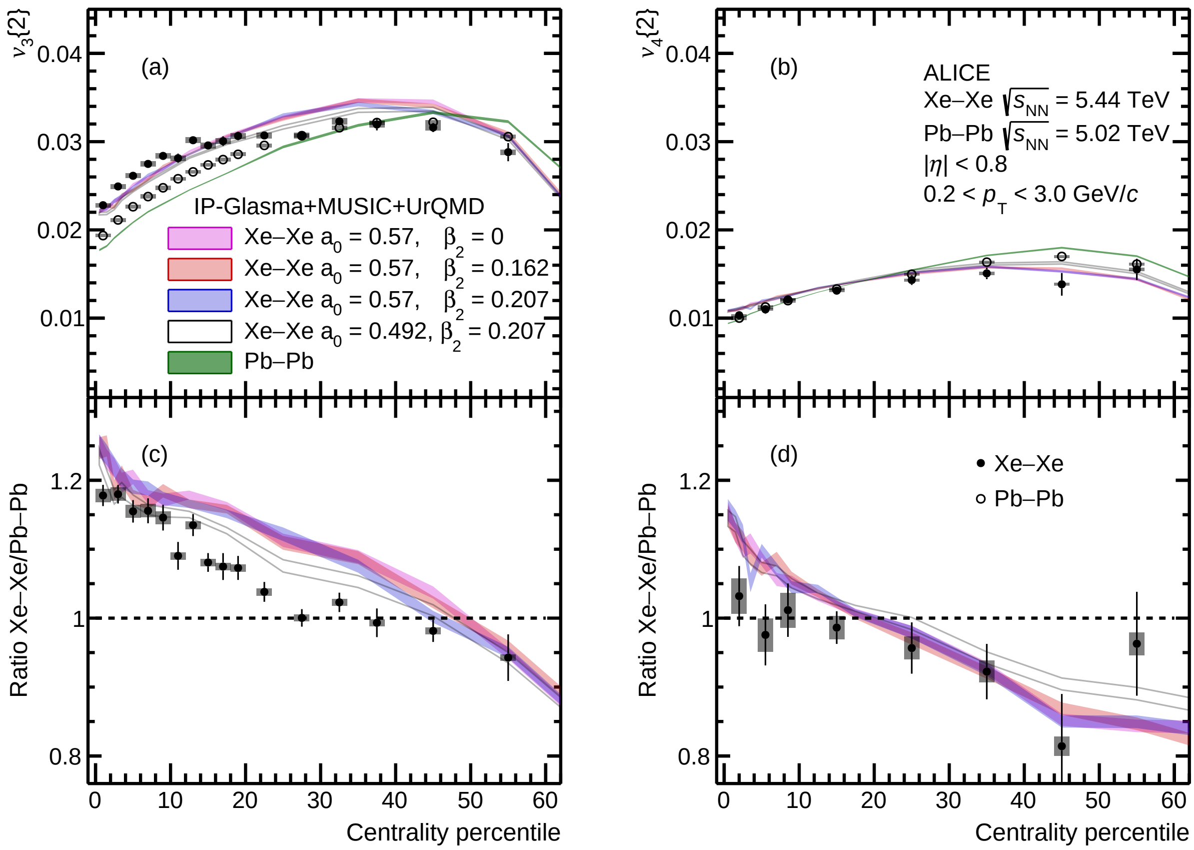

Figure 3: Panels (a) and (b): Charged particle $v_3\{2,|\Delta\eta|>0.8\}$ (left) and $v_4\{2,|\Delta\eta|>0.8\}$ (right) as a function of centrality in Xe–Xe and Pb–Pb collisions at $\sqrt{s_{\rm NN}}$ = 5.44 TeV and $\sqrt{s_{\rm NN}}$ = 5.02 TeV, respectively. Panels (c) and (d): Ratio between Xe–Xe and Pb–Pb $v_3\{2,|\Delta\eta|>0.8\}$ (left) and $v_4\{2,|\Delta\eta|>0.8\}$ (right). Statistical and systematical uncertainties are shown as vertical lines and gray boxes, respectively. The measurements are compared with IP-Glasma+MUSIC+UrQMD calculations [104, 105] to constrain the β_2 and a_0 parameters of ^{129}Xe nuclei.

as reported from previous AMPT calculations [42, 44]. Unfortunately, the significant uncertainties in the measurements preclude a definitive conclusion as to which model calculation better reproduces them.

Delving into the intricate structure of the higher harmonic flow, both linear and nonlinear flow modes are investigated. Figure 4 shows the centrality dependence of the linear and nonlinear components of $v_4\{2\}$, denoted as $v_4^{\rm L}$ and $v_{4,22}$ respectively, in Xe–Xe and Pb–Pb collisions. It has been established that $v_4^{\rm L}$ and $v_{4,22}$ exhibit distinct sensitivities to nuclear deformation parameters [44]. Specifically, $v_4^{\rm L}$ is predominantly influenced by the initial ε_4, while $v_{4,22}$ originates from the initial ε_2^2. In the upper panels of Fig. 4, it can be seen that $v_{4,22}$ increases from central to peripheral Xe–Xe and Pb–Pb collisions while $v_4^{\rm L}$ increases with centrality percentile up to 20% and thereafter decreases towards more peripheral collisions. The $v_{4,22}$ ratio, shown in panel (d) of Fig. 4, starts at approximately 1.5 in most central collisions and decreases toward more peripheral collisions. The $v_4^{\rm L}$ ratio exhibits a milder centrality dependence, aligning with unity within uncertainties for the 0–40% centrality range, beyond which the uncertainties increase considerably. In comparison to the measurements, the IP-Glasma+MUSIC+UrQMD calculations describe $v_{4,22}$ measurements in 0–40% centrality and only marginally overestimate them in 40–60% centrality for Pb–Pb collisions, while they quantitatively capture the $v_{4,22}$ measurements in Xe–Xe collisions. Moreover, nearly all $v_4^{\rm L}$ calculations are slightly above the measurements across the entire centrality range in Fig. 4(a). In Fig. 4(c), the IP-Glasma+MUSIC+UrQMD calculations for $v_4^{\rm L}$ in

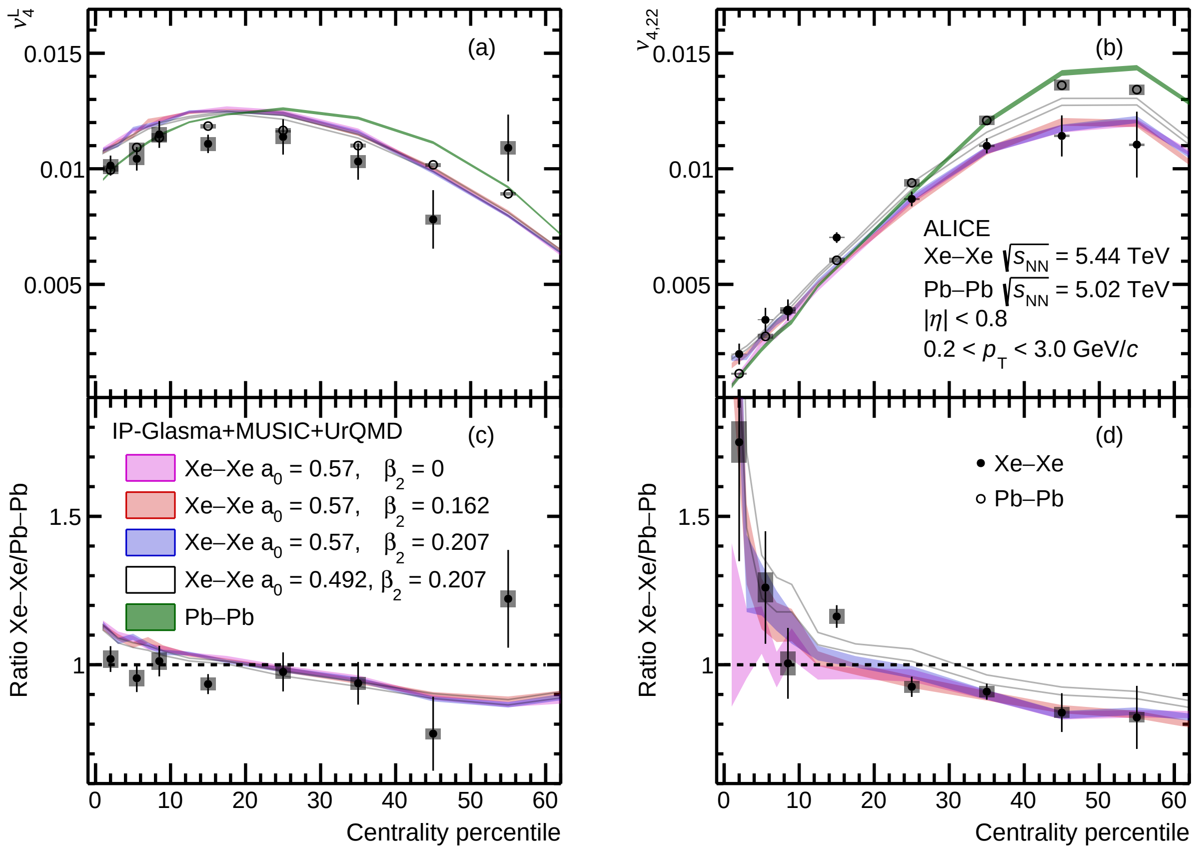

Figure 4: Panels (a) and (b): Charged particle v_4^{L} (left) and $v_{4,22}$ (right) as a function of centrality in Xe–Xe and Pb–Pb collisions at $\sqrt{s_{\mathrm{NN}}}$ = 5.44 TeV and $\sqrt{s_{\mathrm{NN}}}$ = 5.02 TeV, respectively. Panels (c) and (d): Ratio between Xe–Xe and Pb–Pb v_4^{L} (left) and $v_{4,22}$ (right). Statistical and systematical uncertainties are shown as vertical lines and gray boxes, respectively. The measurements are compared with IP-Glasma+MUSIC+UrQMD calculations [104, 105] to constrain the β_2 and a_0 parameters of ^{129}Xe nuclei.

the ratio between Xe–Xe and Pb–Pb are broadly in agreement with the measurements, albeit within the large uncertainties. Regarding the ratios in Fig. 4(d), the measured $v_{4,22}$ ratios in the centrality range 0–20% are better described by the IP-Glasma+MUSIC+UrQMD calculations with a non-zero β_2 and are significantly larger than the one with $\beta_2 = 0$. This aligns with expectations, as $v_{4,22}$ is primarily affected by ε_2^2 in central collisions [41] where ε_2 is influenced mainly by the nuclear quadrupole deformation β_2. Additionally, $v_{4,22}$ ratio calculations using $a_0 = 0.57$ describe the measurements in 20–60% centrality, whereas the one with $a_0 = 0.492$ overestimates the measured $v_{4,22}$ ratio. A similar observation on the sensitivity of $v_{4,22}$ to a_0 in midcentral collisions has been reported in the AMPT studies [44], suggesting that $v_{4,22}$ serves as a promising probe to the nuclear diffuseness.

In addition to the linear and nonlinear flow modes, which depend on the magnitudes of v_2 and/or v_3, the nonlinear coefficient $\chi_{4,22}$ and the symmetry plane correlation $\rho_{4,22}$ are investigated in Xe–Xe and Pb–Pb collisions. Both $\chi_{4,22}$ and $\rho_{4,22}$ have been identified as carrying unique sensitivities to the initial conditions of heavy-ion collisions, rendering them valuable probes for the nuclear structure [66, 68]. The measurements of $\chi_{4,22}$ and $\rho_{4,22}$ are presented as a function of centrality in Fig. 5. Panel (a) shows that $\chi_{4,22}$ measurements in both Xe–Xe and Pb–Pb collisions exhibit a modest centrality dependence, with hints of a finer structure in the most central collisions. The $\chi_{4,22}$ ratio in panel (c) is roughly compatible with unity, albeit with significant uncertainties. In panel (b), $\rho_{4,22}$ shows an increase from central to peripheral collisions in both Xe–Xe and Pb–Pb collisions. The $\rho_{4,22}$ ratio drops steeply in

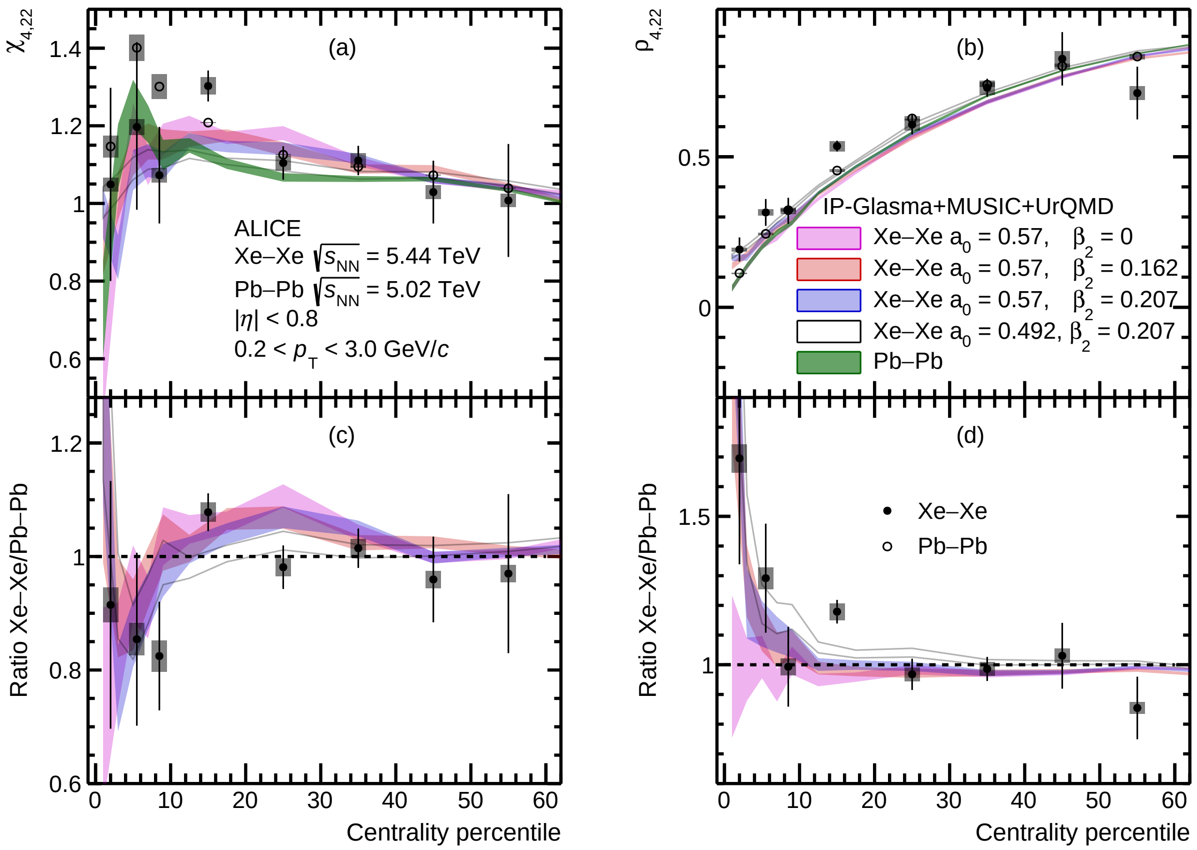

Figure 5: Panels (a) and (b): Charged particle $\chi_{4,22}$ (left) and $\rho_{4,22}$ (right) as a function of centrality in Xe–Xe and Pb–Pb collisions at $\sqrt{s_{\rm NN}}$ = 5.44 TeV and $\sqrt{s_{\rm NN}}$ = 5.02 TeV, respectively. Panels (c) and (d): Ratio between Xe–Xe and Pb–Pb $\chi_{4,22}$ (left) and $\rho_{4,22}$ (right). Statistical and systematical uncertainties are shown as vertical lines and gray boxes, respectively. The measurements are compared with IP-Glasma+MUSIC+UrQMD calculations [104, 105] to constrain the β_2 and a_0 parameters of ^{129}Xe nuclei.

the most central collisions, starting from approximately 1.7 down to unity for centralities above 20%. The IP-Glasma+MUSIC+UrQMD calculations generally capture the centrality dependence of the $\chi_{4,22}$ measurements in both collision systems, with a slight underestimation of the Pb–Pb measurements in the most central collisions. The calculations across different nuclear structure parameters show no marked distinction in the Xe–Xe results. Regarding the ratio of $\rho_{4,22}$ presented in panel (d), the IP-Glasma+MUSIC+UrQMD calculations offer a reasonable description of the measurements, except for the scenario with $\beta_2 = 0$ in the most central collisions, which assumes a spherical ^{129}Xe shape and misses the measured $\rho_{4,22}$ ratio. The pronounced correlations between second and fourth-order symmetry planes, Ψ_2 and Ψ_4, in Xe–Xe collision, are primarily ascribed to the shape of the colliding nuclei influencing the overlap region in central collisions. A deformed ^{129}Xe nuclear structure results in an elliptical overlapping region in central collisions, leading to preferred orientations for the symmetry planes rather than random fluctuations, thereby generating stronger correlations between Ψ_2 and Ψ_4 in Xe–Xe collisions than in Pb–Pb collisions. Overall, the IP-Glasma+MUSIC+UrQMD calculations, considering different a_0 values, do not exhibit significant differences in $\rho_{4,22}$, taking into account the considerable uncertainties in the model calculations.

The normalized symmetric cumulant NSC$(3,2)$, which characterizes the correlation between v_3^2 and v_2^2, is not affected by the dynamic evolution of the systems but retains unique information on the correlations between ε_3^2 and ε_2^2 in the initial conditions [65, 69, 89]. This novel sensitivity to the initial

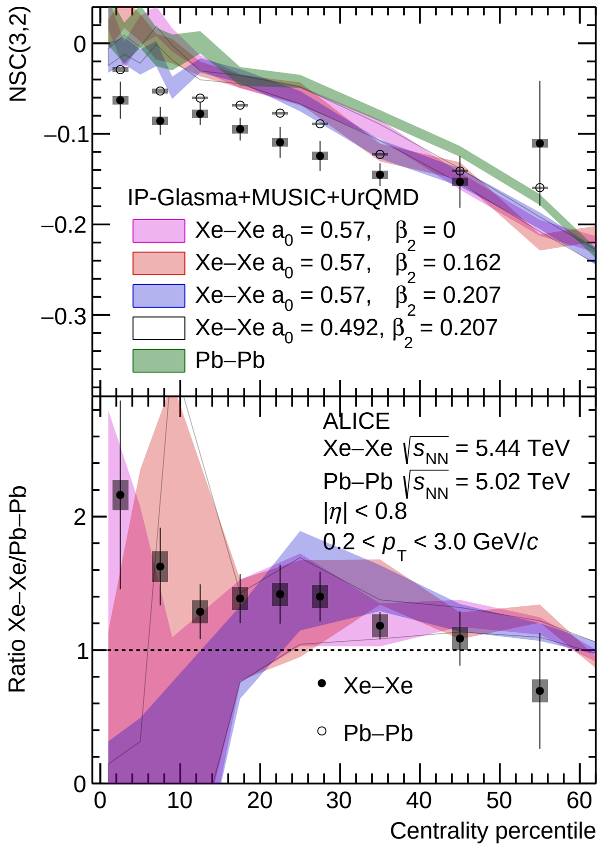

Figure 6: Top Panel: Charged particle NSC(3,2) as a function of centrality in Xe–Xe and Pb–Pb collisions at $\sqrt{s_{\rm NN}}$ = 5.44 TeV and $\sqrt{s_{\rm NN}}$ = 5.02 TeV, respectively. Bottom Panel: Ratio between Xe–Xe and Pb–Pb NSC(3,2). Statistical and systematical uncertainties are shown as vertical lines and gray boxes, respectively. The measurements are compared with IP-Glasma+MUSIC+UrQMD calculations [104, 105] to constrain the β_2 and a_0 parameters of ^{129}Xe nuclei.

geometry renders NSC(3,2) an exemplary probe of nuclear structure, a finding corroborated by AMPT model studies in Ref. [44]. Figure 6 shows the centrality dependence of NSC(3,2) in Xe–Xe and Pb–Pb collisions. The upper panel of Fig. 6 shows that NSC(3,2) decreases from central to peripheral collisions in both collision systems, with the results in Pb–Pb generally larger than those in Xe–Xe. The lower panel presents the NSC(3,2) ratio between Xe–Xe and Pb–Pb, which decreases from central to peripheral collisions for the presented centrality range. The ratio remains above unity for the 0–40% centrality range and then aligns with unity for the 40–60% centrality. The IP-Glasma+MUSIC+UrQMD calculations for NSC(3,2) exceed the measurements in Xe–Xe and Pb–Pb collisions for centralities below 40%; for centralities above 40%, the calculations are approximately consistent with the measured NSC(3,2) within uncertainties. The statistical precision required for calculations of the NSC(3,2) ratio becomes exceedingly challenging in central collisions as NSC(3,2) approaches zero. Although a weak dependence of NSC(3,2) on β_2 was suggested by previous AMPT calculations for Xe–Xe [44] and U–U collisions [42], the IP-Glasma+MUSIC+UrQMD calculations of NSC(3,2) do not demonstrate significant sensitivity to either β_2 or a_0 parameters. More precise theoretical model studies are required to examine the impact of nuclear structure on NSC(3,2).

To quantify the agreement between the experimental measurements and the IP-Glasma+MUSIC+UrQMD

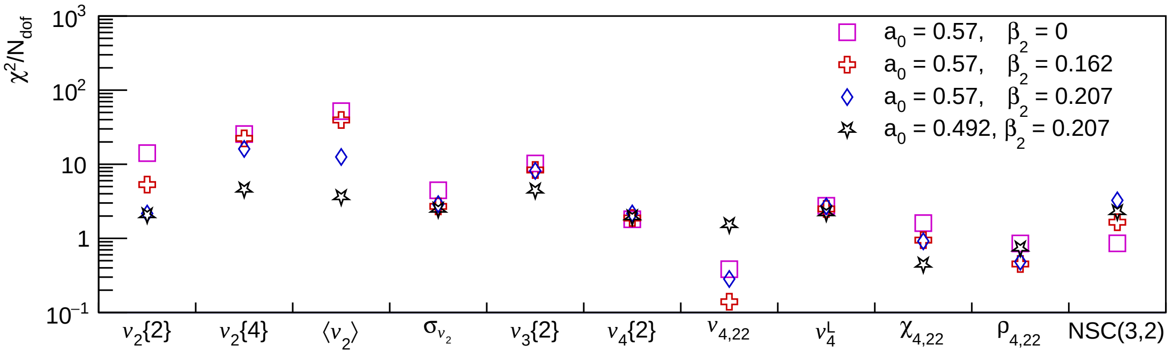

Figure 7: Values of $\chi^2/N_{\rm dof}$ between the measurements (Xe–Xe/Pb–Pb) and the calculations (Xe–Xe/Pb–Pb). The X-axis collects the different measured observables, and the y-axis is shown in a logarithmic scale.

model calculations with the different configurations, a $\chi^2/N_{\rm dof}$ for each observable was calculated as

$$\chi^2/N_{\rm dof} = \frac{1}{N_{\rm dof}} \sum \frac{(y_i - f_i)^2}{\sigma_i^2}, \tag{13}$$

where y_i is the value of the observable experimental measurement at centrality range i and f_i is the value of the observable calculation for the same centrality range with the corresponding configuration, σ_i^2 is the quadratic sum of the statistical uncertainty $\sigma_{\rm stat}$, systematic uncertainty $\sigma_{\rm sys}$, and model uncertainty $\sigma_{\rm model}$. The number of degrees of freedom $N_{\rm dof}$ is obtained by subtracting the number of parameters from the number of data points. Only the measured ratio (Xe–Xe/Pb–Pb) for each observable is considered. The $\chi^2/N_{\rm dof}$ values for the observables considered in this work are shown in Fig. 7. It can be seen that the IP-Glasma+MUSIC+UrQMD calculations with $\beta_2 = 0.207$ generally provide a better description of the measurements of v_2 related observables, as indicated by the smaller $\chi^2/N_{\rm dof}$ values. More specifically, the calculations with $a_0 = 0.492, \beta_2 = 0.207$ yield the smallest $\chi^2/N_{\rm dof}$ for $v_2\{4\}$ and $\langle v_2\rangle$, and result in a consistent $\chi^2/N_{\rm dof}$ in comparison to the calculation using $a_0 = 0.57, \beta_2 = 0.207$ for $v_2\{2, |\Delta\eta| > 1.0\}$ and σ_{v_2}. In addition, the data-to-model $\chi^2/N_{\rm dof}$ values are shown for the $v_3\{2, |\Delta\eta| > 0.8\}$ and v_4 related observables. The IP-Glasma+MUSIC+UrQMD calculations with $a_0 = 0.492$ and $\beta_2 = 0.207$ provide better descriptions of $v_3\{2, |\Delta\eta| > 0.8\}$ and $\chi_{4,22}$, they also perform reasonably well for $v_4\{2, |\Delta\eta| > 0.8\}$ and $\rho_{4,22}$, compared to the calculations using different a_0 or β_2 parameters. In contrast, the calculations with $\beta_2 = 0$ consistently yield relatively poor descriptions, emphasizing the significance of a finite quadrupole deformation for ^{129}Xe. For $v_4\{2, |\Delta\eta| > 0.8\}$ and $v_4^{\rm L}$, all calculations exhibit similar $\chi^2/N_{\rm dof}$ values, aligning with previous discussions that $v_4\{2, |\Delta\eta| > 0.8\}$ and $v_4^{\rm L}$ are not sensitive to the variations in either a_0 or β_2. For $v_{4,22}$, calculations with $a_0 = 0.57$ give the smallest $\chi^2/N_{\rm dof}$ values among all the observables, influenced by the large uncertainties in both the model and the measurements. Such large uncertainties in the 0–10% centrality class limit the ability of $v_{4,22}$ to probe the nuclear shape. Further, as shown in Fig. 7, the calculations with $a_0 = 0.492$ and $\beta_2 = 0.207$ appear to describe the NSC$(3,2)$ measurement well. At the same time, other calculations also yield very small $\chi^2/N_{\rm dof}$ values, attributed to the considerable uncertainties in the NSC(3,2) calculations. Overall, calculations with $\beta_2 = 0.207$ better align with the measurements for the flow observables in Xe–Xe collisions, consistent with the understanding of the deformation of ^{129}Xe from the low-energy nuclear structure studies [19]. The situation is less clear regarding the study of the a_0 parameter of ^{129}Xe. The presented flow measurements demonstrate better overall agreement with the IP-Glasma+MUSIC+UrQMD calculations using $a_0 = 0.492$ compared to $a_0 = 0.57$, with noticeable discrepancies between experimental measurements and IP-Glasma+MUSIC+UrQMD calculations. A definitive answer necessitates a more accurate hydrodynamic model description of the flow measurements. Additional efforts are required to constrain the diffuseness of ^{129}Xe.

5 Summary

The exploration of nuclear structure through multiparticle azimuthal correlations in Xe–Xe collisions at $\sqrt{s_{\rm NN}}$ = 5.44 TeV and Pb–Pb collisions at $\sqrt{s_{\rm NN}}$ = 5.02 TeV at the LHC is presented in this Letter. Systematic measurements of various flow observables, including anisotropic flow coefficients (v_n), flow fluctuations (σ_{v_2}), nonlinear and linear components of flow coefficients ($v_{4,22}$, $v_4^{\rm L}$), nonlinear coefficients ($\chi_{4,22}$), correlations between different symmetry planes ($\rho_{4,22}$), and normalized symmetry cumulants (NSC$(3,2)$), have been performed. Notably, several flow observables exhibit pronounced differences in the ratio between Xe–Xe and Pb–Pb in the most central collisions, which are anticipated from the quadrupole deformation of the ^{129}Xe nuclear structure. Comprehensive comparisons between the experimental measurements and the IP-Glasma+MUSIC+UrQMD calculations are presented to quantify the effects of quadrupole deformation and nuclear diffuseness. Specifically, the calculations employing different β_2 quadrupole deformation parameters and a_0 nuclear diffuseness parameters are discussed. It has been found that among various IP-Glasma+MUSIC+UrQMD model calculations, the one using $\beta_2 = 0.207$ generally provide a better description of the flow measurements. Despite noticeable discrepancies between the measurements and the IP-Glasma+MUSIC+UrQMD predictions, the calculations using $a_0 = 0.492$ seem favored by the presented measurements. Future Bayesian analysis will allow a more robust extraction of the β_2 and a_0 values. The distinct sensitivities of flow observables to β_2 and a_0 offer valuable insights into constraining the deformation and diffuseness of ^{129}Xe in its ground state. The systematic studies using multiparticle azimuthal correlation at the LHC are opening new avenues for the investigation of nuclear structure at the energy frontier, complementing low-energy nuclear structure studies and deepening the knowledge of fundamental nuclear properties. Upcoming ^{16}O–^{16}O collisions at the LHC will provide novel opportunities to explore the full potential of the LHC on the nuclear structure study probing, in particular, for the first time the α-cluster structure of ^{16}O at the TeV energy scale [26, 112–115].

Acknowledgements

The ALICE Collaboration would like to thank Chun Shen and Bjoern Schenke for providing the latest calculations from the state-of-the-art models. The ALICE Collaboration would like to thank all its engineers and technicians for their invaluable contributions to the construction of the experiment and the CERN accelerator teams for the outstanding performance of the LHC complex. The ALICE Collaboration gratefully acknowledges the resources and support provided by all Grid centres and the Worldwide LHC Computing Grid (WLCG) collaboration. The ALICE Collaboration acknowledges the following funding agencies for their support in building and running the ALICE detector: A. I. Alikhanyan National Science Laboratory (Yerevan Physics Institute) Foundation (ANSL), State Committee of Science and World Federation of Scientists (WFS), Armenia; Austrian Academy of Sciences, Austrian Science Fund (FWF): [M 2467-N36] and Nationalstiftung für Forschung, Technologie und Entwicklung, Austria; Ministry of Communications and High Technologies, National Nuclear Research Center, Azerbaijan; Conselho Nacional de Desenvolvimento Científico e Tecnológico (CNPq), Financiadora de Estudos e Projetos (Finep), Fundação de Amparo à Pesquisa do Estado de São Paulo (FAPESP) and Universidade Federal do Rio Grande do Sul (UFRGS), Brazil; Bulgarian Ministry of Education and Science, within the National Roadmap for Research Infrastructures 2020-2027 (object CERN), Bulgaria; Ministry of Education of China (MOEC) , Ministry of Science & Technology of China (MSTC) and National Natural Science Foundation of China (NSFC), China; Ministry of Science and Education and Croatian Science Foundation, Croatia; Centro de Aplicaciones Tecnológicas y Desarrollo Nuclear (CEADEN), Cubaenergía, Cuba; Ministry of Education, Youth and Sports of the Czech Republic, Czech Republic; The Danish Council for Independent Research | Natural Sciences, the VILLUM FONDEN and Danish National Research Foundation (DNRF), Denmark; Helsinki Institute of Physics (HIP), Finland; Commissariat à l'Energie Atomique (CEA) and Institut National de Physique Nucléaire et de Physique des Particules (IN2P3) and Centre National de la Recherche Scientifique (CNRS), France; Bundesministerium für Bildung und Forschung (BMBF) and GSI Helmholtzzentrum für Schwerionenforschung GmbH, Germany; General Secretariat for Research and Technology, Ministry of Education, Research and Religions, Greece; National Research, Development and Innovation Office, Hungary; Department of Atomic Energy Government of India (DAE), Department of Science and Technology, Government of India (DST), University Grants Commission, Government of India (UGC) and Council of Scientific and Industrial Research (CSIR), India; National Research and Innovation Agency - BRIN, Indonesia; Istituto Nazionale di Fisica Nucleare (INFN), Italy; Japanese Ministry of Education, Culture, Sports, Science and Technology (MEXT) and Japan Society for the Promotion of Science (JSPS) KAKENHI, Japan; Consejo Nacional de Ciencia (CONACYT) y Tecnología, through Fondo de Cooperación Internacional en Ciencia y Tecnología (FONCICYT) and Dirección General de Asuntos del Personal Academico (DGAPA), Mexico; Nederlandse Organisatie voor Wetenschappelijk Onderzoek (NWO), Netherlands; The Research Council of Norway, Norway; Pontificia Universidad Católica del Perú, Peru; Ministry of Science and Higher Education, National Science Centre and WUT ID-UB, Poland; Korea Institute of Science and Technology Information and National Research Foundation of Korea (NRF), Republic of Korea; Ministry of Education and Scientific Research, Institute of Atomic Physics, Ministry of Research and Innovation and Institute of Atomic Physics and Universitatea Nationala de Stiinta si Tehnologie Politehnica Bucuresti, Romania; Ministry of Education, Science, Research and Sport of the Slovak Republic, Slovakia; National Research Foundation of South Africa, South Africa; Swedish Research Council (VR) and Knut & Alice Wallenberg Foundation (KAW), Sweden; European Organization for Nuclear Research, Switzerland; Suranaree University of Technology (SUT), National Science and Technology Development Agency (NSTDA) and National Science, Research and Innovation Fund (NSRF via PMU-B B05F650021), Thailand; Turkish Energy, Nuclear and Mineral Research Agency (TENMAK), Turkey; National Academy of Sciences of Ukraine, Ukraine; Science and Technology Facilities Council (STFC), United Kingdom; National Science Foundation of the United States of America (NSF) and United States Department of Energy, Office of Nuclear Physics (DOE NP), United States of America. In addition, individual groups or members have received support from: Czech Science Foundation (grant no. 23-07499S), Czech Republic; FORTE project, reg. no. CZ.02.01.01/00/22_008/0004632, Czech Republic, co-funded by the European Union, Czech Republic; European Research Council (grant no. 950692), European Union; ICSC - Centro Nazionale di Ricerca in High Performance Computing, Big Data and Quantum Computing, European Union - NextGenerationEU; Academy of Finland (Center of Excellence in Quark Matter) (grant nos. 346327, 346328), Finland.

References

[1] H. Hergert, "A Guided Tour of *ab initio* Nuclear Many-Body Theory", *Front. in Phys.* **8** (2020) 379, `arXiv:2008.05061 [nucl-th]`.

[2] S. Gandolfi, D. Lonardoni, A. Lovato, and M. Piarulli, "Atomic nuclei from quantum Monte Carlo calculations with chiral EFT interactions", *Front. in Phys.* **8** (2020) 117, `arXiv:2001.01374 [nucl-th]`.

[3] V. Somà, "Self-consistent Green's function theory for atomic nuclei", *Front. in Phys.* **8** (2020) 340, `arXiv:2003.11321 [nucl-th]`.

[4] T. A. Lähde and U.-G. Meißner, *Nuclear Lattice Effective Field Theory: An introduction*, vol. 957. Springer, 2019.

[5] A. Ekström, C. Forssén, G. Hagen, G. R. Jansen, W. Jiang, and T. Papenbrock, "What is ab initio in nuclear theory?", *Front. Phys.* **11** (2023) 1129094, `arXiv:2212.11064 [nucl-th]`.

[6] V. Lapoux, V. Somà, C. Barbieri, H. Hergert, J. D. Holt, and S. R. Stroberg, "Radii and Binding Energies in Oxygen Isotopes: A Challenge for Nuclear Forces", *Phys. Rev. Lett.* **117** (2016) 052501, `arXiv:1605.07885 [nucl-ex]`.

[7] D. Lonardoni, J. Carlson, S. Gandolfi, J. E. Lynn, K. E. Schmidt, A. Schwenk, and X. Wang, "Properties of nuclei up to $A = 16$ using local chiral interactions", *Phys. Rev. Lett.* **120** (2018) 122502, `arXiv:1709.09143 [nucl-th]`.

[8] S. J. Novario, G. Hagen, G. R. Jansen, and T. Papenbrock, "Charge radii of exotic neon and magnesium isotopes", *Phys. Rev. C* **102** (2020) 051303, `arXiv:2007.06684 [nucl-th]`.

[9] A. Koszorús *et al.*, "Charge radii of exotic potassium isotopes challenge nuclear theory and the magic character of $N = 32$", *Nature Phys.* **17** (2021) 439–443, `arXiv:2012.01864 [nucl-ex]`. [Erratum: Nature Phys. 17, 539 (2021)].

[10] H. Heylen *et al.*, "High-resolution laser spectroscopy of $^{27-32}$Al", *Phys. Rev. C* **103** (2021) 014318, `arXiv:2010.06918 [nucl-ex]`.

[11] B. Ohayon, R. F. G. Ruiz, Z. H. Sun, G. Hagen, T. Papenbrock, and B. K. Sahoo, "Nuclear charge radii of Na isotopes: Interplay of atomic and nuclear theory", *Phys. Rev. C* **105** (2022) L031305, `arXiv:2109.10539 [physics.atom-ph]`.

[12] V. Somà, P. Navrátil, F. Raimondi, C. Barbieri, and T. Duguet, "Novel chiral Hamiltonian and observables in light and medium-mass nuclei", *Phys. Rev. C* **101** (2020) 014318, `arXiv:1907.09790 [nucl-th]`.

[13] Z. T. Lu, P. Mueller, G. W. F. Drake, W. Noertershaeuser, S. C. Pieper, and Z. C. Yan, "Colloquium: Laser probing of neutron-rich nuclei in light atoms", *Rev. Mod. Phys.* **85** (2013) 1383–1400, `arXiv:1307.2872 [nucl-ex]`.

[14] B. Maaß *et al.*, "Nuclear Charge Radii of ^{10,11}B", *Phys. Rev. Lett.* **122** (2019) 182501, `arXiv:1901.06323 [physics.atom-ph]`.

[15] **PREX** Collaboration, D. Adhikari *et al.*, "Accurate Determination of the Neutron Skin Thickness of ^{208}Pb through Parity-Violation in Electron Scattering", *Phys. Rev. Lett.* **126** (2021) 172502, `arXiv:2102.10767 [nucl-ex]`.

[16] **CREX** Collaboration, D. Adhikari *et al.*, "Precision Determination of the Neutral Weak Form Factor of Ca48", *Phys. Rev. Lett.* **129** (2022) 042501, `arXiv:2205.11593 [nucl-ex]`.

[17] C. A. Bertulani and J. Valencia, "Neutron skins as laboratory constraints on properties of neutron stars and on what we can learn from heavy ion fragmentation reactions", *Phys. Rev. C* **100** (2019) 015802, `arXiv:1904.01078 [nucl-th]`.

[18] G. Giacalone, G. Nijs, and W. van der Schee, "Determination of the Neutron Skin of ^{208}Pb from Ultrarelativistic Nuclear Collisions", *Phys. Rev. Lett.* **131** (2023) 202302, `arXiv:2305.00015 [nucl-th]`.

[19] B. Bally, G. Giacalone, and M. Bender, "Structure of ^{128,129,130}Xe through multi-reference energy density functional calculations", *Eur. Phys. J. A* **58** (2022) 187, `arXiv:2207.13576 [nucl-th]`.

[20] Y. L. Yang, P. W. Zhao, and Z. P. Li, "Shape and multiple shape coexistence of nuclei within covariant density functional theory", *Phys. Rev. C* **107** (2023) 024308, `arXiv:2302.07417 [nucl-th]`.

[21] S. Shen, S. Elhatisari, T. A. Lähde, D. Lee, B.-N. Lu, and U.-G. Meißner, "Emergent geometry and duality in the carbon nucleus", *Nature Commun.* **14** (2023) 2777, arXiv:2202.13596 [nucl-th].

[22] **STAR** Collaboration, L. Adamczyk *et al.*, "Azimuthal anisotropy in U+U and Au+Au collisions at RHIC", *Phys. Rev. Lett.* **115** (2015) 222301, arXiv:1505.07812 [nucl-ex].

[23] **STAR** Collaboration, M. Abdallah *et al.*, "Search for the chiral magnetic effect with isobar collisions at $\sqrt{s_{\mathrm{NN}}}$=200 GeV by the STAR Collaboration at the BNL Relativistic Heavy Ion Collider", *Phys. Rev. C* **105** (2022) 014901, arXiv:2109.00131 [nucl-ex].

[24] C. Zhang and J. Jia, "Evidence of Quadrupole and Octupole Deformations in ^{96}Zr+^{96}Zr and ^{96}Ru+^{96}Ru Collisions at Ultrarelativistic Energies", *Phys. Rev. Lett.* **128** (2022) 022301, arXiv:2109.01631 [nucl-th].

[25] **STAR** Collaboration, "Imaging Shapes of Atomic Nuclei in High-Energy Nuclear Collisions", arXiv:2401.06625 [nucl-ex].

[26] X.-L. Zhao, G.-L. Ma, Y. Zhou, Z.-W. Lin, and C. Zhang, "Nuclear cluster structure effect in ^{16}O+^{16}O collisions at the top RHIC energy", arXiv:2404.09780 [nucl-th].

[27] **ALICE** Collaboration, S. Acharya *et al.*, "Anisotropic flow in Xe-Xe collisions at $\sqrt{s_{\mathrm{NN}}} = 5.44$ TeV", *Phys. Lett. B* **784** (2018) 82–95, arXiv:1805.01832 [nucl-ex].

[28] **ALICE** Collaboration, S. Acharya *et al.*, "Centrality determination using the Glauber model in Xe-Xe collisions at $\sqrt{s_{\mathrm{NN}}} = 5.44$ TeV", ALICE-PUBLIC-2018-003. https://cds.cern.ch/record/2315401.

[29] **ALICE** Collaboration, S. Acharya *et al.*, "Centrality and pseudorapidity dependence of the charged-particle multiplicity density in Xe–Xe collisions at $\sqrt{s_{\mathrm{NN}}} = 5.44$ TeV", *Phys. Lett. B* **790** (2019) 35–48, arXiv:1805.04432 [nucl-ex].

[30] **ATLAS** Collaboration, G. Aad *et al.*, "Correlations between flow and transverse momentum in Xe+Xe and Pb+Pb collisions at the LHC with the ATLAS detector: A probe of the heavy-ion initial state and nuclear deformation", *Phys. Rev. C* **107** (2023) 054910, arXiv:2205.00039 [nucl-ex].

[31] **CMS** Collaboration, A. M. Sirunyan *et al.*, "Charged-particle angular correlations in XeXe collisions at $\sqrt{s_{\mathrm{NN}}} = 5.44$ TeV", *Phys. Rev. C* **100** (2019) 044902, arXiv:1901.07997 [hep-ex].

[32] G. Giacalone, J. Jia, and C. Zhang, "Impact of Nuclear Deformation on Relativistic Heavy-Ion Collisions: Assessing Consistency in Nuclear Physics across Energy Scales", *Phys. Rev. Lett.* **127** (2021) 242301, arXiv:2105.01638 [nucl-th].

[33] S. Zhao, H.-j. Xu, Y.-X. Liu, and H. Song, "Probing the nuclear deformation with three-particle asymmetric cumulant in RHIC isobar runs", *Phys. Lett. B* **839** (2023) 137838, arXiv:2204.02387 [nucl-th].

[34] **ALICE** Collaboration, S. Acharya *et al.*, "Characterizing the initial conditions of heavy-ion collisions at the LHC with mean transverse momentum and anisotropic flow correlations", *Phys. Lett. B* **834** (2022) 137393, arXiv:2111.06106 [nucl-ex].

[35] B. Bally, M. Bender, G. Giacalone, and V. Somà, "Evidence of the triaxial structure of ^{129}Xe at the Large Hadron Collider", *Phys. Rev. Lett.* **128** (2022) 082301, arXiv:2108.09578 [nucl-th].

[36] H.-j. Xu, J. Zhao, and F. Wang, "Hexadecapole Deformation of U238 from Relativistic Heavy-Ion Collisions Using a Nonlinear Response Coefficient", *Phys. Rev. Lett.* **132** (2024) 262301, `arXiv:2402.16550 [nucl-th]`.

[37] W. Ryssens, G. Giacalone, B. Schenke, and C. Shen, "Evidence of Hexadecapole Deformation in Uranium-238 at the Relativistic Heavy Ion Collider", *Phys. Rev. Lett.* **130** (2023) 212302, `arXiv:2302.13617 [nucl-th]`.

[38] H. Li, H.-j. Xu, Y. Zhou, X. Wang, J. Zhao, L.-W. Chen, and F. Wang, "Probing the neutron skin with ultrarelativistic isobaric collisions", *Phys. Rev. Lett.* **125** (2020) 222301, `arXiv:1910.06170 [nucl-th]`.

[39] H.-j. Xu, W. Zhao, H. Li, Y. Zhou, L.-W. Chen, and F. Wang, "Probing nuclear structure with mean transverse momentum in relativistic isobar collisions", *Phys. Rev. C* **108** (2023) L011902, `arXiv:2111.14812 [nucl-th]`.

[40] J. Jia, "Probing triaxial deformation of atomic nuclei in high-energy heavy ion collisions", *Phys. Rev. C* **105** (2022) 044905, `arXiv:2109.00604 [nucl-th]`.

[41] J. Jia, "Shape of atomic nuclei in heavy ion collisions", *Phys. Rev. C* **105** (2022) 014905, `arXiv:2106.08768 [nucl-th]`.

[42] N. Magdy, "Impact of nuclear deformation on collective flow observables in relativistic U+U collisions", *Eur. Phys. J. A* **59** (2023) 64, `arXiv:2206.05332 [nucl-th]`.

[43] E. G. D. Nielsen, F. K. Rømer, K. Gulbrandsen, and Y. Zhou, "Generic multi-particle transverse momentum correlations as a new tool for studying nuclear structure at the energy frontier", *Eur. Phys. J. A* **60** (2024) 38, `arXiv:2312.00492 [nucl-th]`.

[44] Z. Lu, M. Zhao, X. Li, J. Jia, and Y. Zhou, "Probe nuclear structure using the anisotropic flow at the Large Hadron Collider", *Eur. Phys. J. A* **59** (2023) 279, `arXiv:2309.09663 [nucl-th]`.

[45] S. Zhao, H.-j. Xu, Y. Zhou, Y.-X. Liu, and H. Song, "Exploring the Nuclear Shape Phase Transition in Ultra-Relativistic ^{129}Xe+^{129}Xe Collisions at the LHC", `arXiv:2403.07441 [nucl-th]`.

[46] B. Muller, J. Schukraft, and B. Wyslouch, "First Results from Pb+Pb collisions at the LHC", *Ann. Rev. Nucl. Part. Sci.* **62** (2012) 361–386, `arXiv:1202.3233 [hep-ex]`.

[47] H.-J. Drescher, A. Dumitru, C. Gombeaud, and J.-Y. Ollitrault, "The Centrality dependence of elliptic flow, the hydrodynamic limit, and the viscosity of hot QCD", *Phys. Rev. C* **76** (2007) 024905, `arXiv:0704.3553 [nucl-th]`.

[48] U. Heinz and R. Snellings, "Collective flow and viscosity in relativistic heavy-ion collisions", *Ann. Rev. Nucl. Part. Sci.* **63** (2013) 123–151, `arXiv:1301.2826 [nucl-th]`.

[49] D. Molnar and M. Gyulassy, "Saturation of elliptic flow and the transport opacity of the gluon plasma at RHIC", *Nucl. Phys. A* **697** (2002) 495–520, `arXiv:nucl-th/0104073`. [Erratum: Nucl.Phys.A 703, 893–894 (2002)].

[50] H. Song, Y. Zhou, and K. Gajdosova, "Collective flow and hydrodynamics in large and small systems at the LHC", *Nucl. Sci. Tech.* **28** (2017) 99, `arXiv:1703.00670 [nucl-th]`.

[51] **ALICE** Collaboration, S. Acharya *et al.*, "The ALICE experiment: a journey through QCD", *Eur. Phys. J. C* **84** (2024) 813, `arXiv:2211.04384 [nucl-ex]`.

[52] S. Voloshin and Y. Zhang, "Flow study in relativistic nuclear collisions by Fourier expansion of Azimuthal particle distributions", *Z. Phys. C* **70** (1996) 665–672, `arXiv:hep-ph/9407282`.

[53] **ALICE** Collaboration, K. Aamodt *et al.*, "Higher harmonic anisotropic flow measurements of charged particles in Pb–Pb collisions at $\sqrt{s_{\mathrm{NN}}} = 2.76$ TeV", *Phys. Rev. Lett.* **107** (2011) 032301, `arXiv:1105.3865 [nucl-ex]`.

[54] **ALICE** Collaboration, J. Adam *et al.*, "Anisotropic flow of charged particles in Pb–Pb collisions at $\sqrt{s_{\mathrm{NN}}} = 5.02$ TeV", *Phys. Rev. Lett.* **116** (2016) 132302, `arXiv:1602.01119 [nucl-ex]`.

[55] **ALICE** Collaboration, S. Acharya *et al.*, "Investigations of Anisotropic Flow Using Multiparticle Azimuthal Correlations in pp, p–Pb, Xe–Xe, and Pb–Pb Collisions at the LHC", *Phys. Rev. Lett.* **123** (2019) 142301, `arXiv:1903.01790 [nucl-ex]`.

[56] **ATLAS** Collaboration, G. Aad *et al.*, "Measurement of the azimuthal anisotropy for charged particle production in $\sqrt{s_{\mathrm{NN}}} = 2.76$ TeV lead-lead collisions with the ATLAS detector", *Phys. Rev. C* **86** (2012) 014907, `arXiv:1203.3087 [hep-ex]`.

[57] **ATLAS** Collaboration, G. Aad *et al.*, "Measurement of the azimuthal anisotropy of charged-particle production in Xe+Xe collisions at $\sqrt{s_{\mathrm{NN}}} = 5.44$ TeV with the ATLAS detector", *Phys. Rev. C* **101** (2020) 024906, `arXiv:1911.04812 [nucl-ex]`.

[58] **CMS** Collaboration, S. Chatrchyan *et al.*, "Measurement of Higher-Order Harmonic Azimuthal Anisotropy in PbPb Collisions at $\sqrt{s_{\mathrm{NN}}} = 2.76$ TeV", *Phys. Rev. C* **89** (2014) 044906, `arXiv:1310.8651 [nucl-ex]`.

[59] **ALICE** Collaboration, S. Acharya *et al.*, "Energy dependence and fluctuations of anisotropic flow in Pb–Pb collisions at $\sqrt{s_{\mathrm{NN}}} = 5.02$ and 2.76 TeV", *JHEP* **07** (2018) 103, `arXiv:1804.02944 [nucl-ex]`.

[60] **ALICE** Collaboration, S. Acharya *et al.*, "Observation of flow angle and flow magnitude fluctuations in Pb-Pb collisions at $\sqrt{s_{\mathrm{NN}}}$ =5.02TeV at the CERN Large Hadron Collider", *Phys. Rev. C* **107** (2023) L051901, `arXiv:2206.04574 [nucl-ex]`.

[61] **ALICE** Collaboration, S. Acharya *et al.*, "Systematic study of flow vector fluctuations in $\sqrt{s_{\mathrm{NN}}}$ =5.02 TeV Pb-Pb collisions", *Phys. Rev. C* **109** (2024) 065202, `arXiv:2403.15213 [nucl-ex]`.

[62] **ALICE** Collaboration, S. Acharya *et al.*, "Pseudorapidity dependence of anisotropic flow and its decorrelations using long-range multiparticle correlations in Pb–Pb and Xe–Xe collisions", *Phys. Lett. B* **850** (2024) 138477, `arXiv:2307.11116 [nucl-ex]`. [Erratum: Phys.Lett.B 853, 138659 (2024)].

[63] **ATLAS** Collaboration, G. Aad *et al.*, "Measurement of the distributions of event-by-event flow harmonics in lead-lead collisions at $\sqrt{s_{\mathrm{NN}}} = 2.76$ TeV with the ATLAS detector at the LHC", *JHEP* **11** (2013) 183, `arXiv:1305.2942 [hep-ex]`.

[64] **CMS** Collaboration, A. M. Sirunyan *et al.*, "Non-Gaussian elliptic-flow fluctuations in PbPb collisions at $\sqrt{s_{\mathrm{NN}}} = 5.02$ TeV", *Phys. Lett. B* **789** (2019) 643–665, `arXiv:1711.05594 [nucl-ex]`.

[65] **ALICE** Collaboration, J. Adam *et al.*, "Correlated event-by-event fluctuations of flow harmonics in Pb–Pb collisions at $\sqrt{s_{\mathrm{NN}}} = 2.76$ TeV", *Phys. Rev. Lett.* **117** (2016) 182301, `arXiv:1604.07663 [nucl-ex]`.

[66] **ALICE** Collaboration, S. Acharya *et al.*, “Linear and non-linear flow modes in Pb–Pb collisions at $\sqrt{s_{\rm NN}} = 2.76$ TeV”, *Phys. Lett. B* **773** (2017) 68–80, arXiv:1705.04377 [nucl-ex].

[67] **ALICE** Collaboration, S. Acharya *et al.*, “Systematic studies of correlations between different order flow harmonics in Pb–Pb collisions at $\sqrt{s_{\rm NN}} = 2.76$ TeV”, *Phys. Rev. C* **97** (2018) 024906, arXiv:1709.01127 [nucl-ex].

[68] **ALICE** Collaboration, S. Acharya *et al.*, “Higher harmonic non-linear flow modes of charged hadrons in Pb–Pb collisions at $\sqrt{s_{\rm NN}} = 5.02$ TeV”, *JHEP* **05** (2020) 085, arXiv:2002.00633 [nucl-ex].

[69] **ALICE** Collaboration, S. Acharya *et al.*, “Measurements of mixed harmonic cumulants in Pb–Pb collisions at $\sqrt{s_{\rm NN}} = 5.02$ TeV”, *Phys. Lett. B* **818** (2021) 136354, arXiv:2102.12180 [nucl-ex].

[70] **ATLAS** Collaboration, G. Aad *et al.*, “Measurement of the correlation between flow harmonics of different order in lead-lead collisions at $\sqrt{s_{\rm NN}} = 2.76$ TeV with the ATLAS detector”, *Phys. Rev. C* **92** (2015) 034903, arXiv:1504.01289 [hep-ex].

[71] K. Hagino, N. W. Lwin, and M. Yamagami, “Deformation parameter for diffuse density”, *Phys. Rev. C* **74** (2006) 017310, arXiv:nucl-th/0604048.

[72] S. Raman, C. W. G. Nestor, Jr, and P. Tikkanen, “Transition probability from the ground to the first-excited 2^+ state of even-even nuclides”, *Atom. Data Nucl. Data Tabl.* **78** (2001) 1–128.

[73] B. Pritychenko, M. Birch, B. Singh, and M. Horoi, “Tables of E2 Transition Probabilities from the first 2^+ States in Even-Even Nuclei”, *Atom. Data Nucl. Data Tabl.* **107** (2016) 1–139, arXiv:1312.5975 [nucl-th]. [Erratum: Atom.Data Nucl.Data Tabl. 114, 371–374 (2017)].

[74] A. Bilandzic, C. H. Christensen, K. Gulbrandsen, A. Hansen, and Y. Zhou, “Generic framework for anisotropic flow analyses with multiparticle azimuthal correlations”, *Phys. Rev. C* **89** (2014) 064904, arXiv:1312.3572 [nucl-ex].

[75] A. Bilandzic, R. Snellings, and S. Voloshin, “Flow analysis with cumulants: Direct calculations”, *Phys. Rev. C* **83** (2011) 044913, arXiv:1010.0233 [nucl-ex].

[76] N. Borghini, P. M. Dinh, and J.-Y. Ollitrault, “A New method for measuring azimuthal distributions in nucleus-nucleus collisions”, *Phys. Rev. C* **63** (2001) 054906, arXiv:nucl-th/0007063.

[77] Z. Moravcova, K. Gulbrandsen, and Y. Zhou, “Generic algorithm for multiparticle cumulants of azimuthal correlations in high energy nucleus collisions”, *Phys. Rev. C* **103** (2021) 024913, arXiv:2005.07974 [nucl-th].

[78] S. A. Voloshin, A. M. Poskanzer, A. Tang, and G. Wang, “Elliptic flow in the Gaussian model of eccentricity fluctuations”, *Phys. Lett. B* **659** (2008) 537–541, arXiv:0708.0800 [nucl-th].

[79] H. Niemi, G. S. Denicol, H. Holopainen, and P. Huovinen, “Event-by-event distributions of azimuthal asymmetries in ultrarelativistic heavy-ion collisions”, *Phys. Rev. C* **87** (2013) 054901, arXiv:1212.1008 [nucl-th].

[80] H. Song, S. A. Bass, U. Heinz, T. Hirano, and C. Shen, “200 A GeV Au+Au collisions serve a nearly perfect quark-gluon liquid”, *Phys. Rev. Lett.* **106** (2011) 192301, arXiv:1011.2783 [nucl-th]. [Erratum: Phys.Rev.Lett. 109, 139904 (2012)].

[81] B. Alver and G. Roland, "Collision geometry fluctuations and triangular flow in heavy-ion collisions", *Phys. Rev. C* **81** (2010) 054905, arXiv:1003.0194 [nucl-th]. [Erratum: Phys.Rev.C 82, 039903 (2010)].

[82] R. S. Bhalerao, J.-Y. Ollitrault, and S. Pal, "Characterizing flow fluctuations with moments", *Phys. Lett. B* **742** (2015) 94–98, arXiv:1411.5160 [nucl-th].

[83] R. S. Bhalerao, J.-Y. Ollitrault, and S. Pal, "Event-plane correlators", *Phys. Rev. C* **88** (2013) 024909, arXiv:1307.0980 [nucl-th].

[84] L. Yan and J.-Y. Ollitrault, "v_4, v_5, v_6, v_7: nonlinear hydrodynamic response versus LHC data", *Phys. Lett. B* **744** (2015) 82–87, arXiv:1502.02502 [nucl-th].

[85] Y. Zhou, K. Xiao, Z. Feng, F. Liu, and R. Snellings, "Anisotropic distributions in a multiphase transport model", *Phys. Rev. C* **93** (2016) 034909, arXiv:1508.03306 [nucl-ex].

[86] J. Qian, U. W. Heinz, and J. Liu, "Mode-coupling effects in anisotropic flow in heavy-ion collisions", *Phys. Rev. C* **93** (2016) 064901, arXiv:1602.02813 [nucl-th].

[87] J. E. Parkkila, A. Onnerstad, and D. J. Kim, "Bayesian estimation of the specific shear and bulk viscosity of the quark-gluon plasma with additional flow harmonic observables", *Phys. Rev. C* **104** (2021) 054904, arXiv:2106.05019 [hep-ph].

[88] J. E. Parkkila, A. Onnerstad, S. F. Taghavi, C. Mordasini, A. Bilandzic, M. Virta, and D. J. Kim, "New constraints for QCD matter from improved Bayesian parameter estimation in heavy-ion collisions at LHC", *Phys. Lett. B* **835** (2022) 137485, arXiv:2111.08145 [hep-ph].

[89] X. Zhu, Y. Zhou, H. Xu, and H. Song, "Correlations of flow harmonics in 2.76A TeV Pb–Pb collisions", *Phys. Rev. C* **95** (2017) 044902, arXiv:1608.05305 [nucl-th].

[90] P. Huo, K. Gajdošová, J. Jia, and Y. Zhou, "Importance of non-flow in mixed-harmonic multi-particle correlations in small collision systems", *Phys. Lett. B* **777** (2018) 201–206, arXiv:1710.07567 [nucl-ex].

[91] **ALICE** Collaboration, B. B. Abelev *et al.*, "Multiparticle azimuthal correlations in p–Pb and Pb–Pb collisions at the CERN Large Hadron Collider", *Phys. Rev. C* **90** (2014) 054901, arXiv:1406.2474 [nucl-ex].

[92] **ALICE** Collaboration, K. Aamodt *et al.*, "The ALICE experiment at the CERN LHC", *JINST* **3** (2008) S08002.

[93] **ALICE** Collaboration, P. Cortese *et al.*, "ALICE: Physics performance report, volume I", *J. Phys. G* **30** (2004) 1517–1763.

[94] **ALICE** Collaboration, C. W. Fabjan *et al.*, "ALICE: Physics Performance Report, volume II", *J. Phys. G* **32** (2006) 1295–2040.

[95] **ALICE** Collaboration, B. B. Abelev *et al.*, "Performance of the ALICE Experiment at the CERN LHC", *Int. J. Mod. Phys. A* **29** (2014) 1430044, arXiv:1402.4476 [nucl-ex].

[96] **ALICE** Collaboration, E. Abbas *et al.*, "Performance of the ALICE VZERO system", *JINST* **8** (2013) P10016, arXiv:1306.3130 [nucl-ex].

[97] **ALICE** Collaboration, K. Aamodt *et al.*, "Alignment of the ALICE Inner Tracking System with cosmic-ray tracks", *JINST* **5** (2010) P03003, arXiv:1001.0502 [physics.ins-det].

[98] J. Alme *et al.*, “The ALICE TPC, a large 3-dimensional tracking device with fast readout for ultra-high multiplicity events”, *Nucl. Instrum. Meth. A* **622** (2010) 316–367, arXiv:1001.1950 [physics.ins-det].

[99] **ALICE** Collaboration, B. Abelev *et al.*, “Centrality determination of Pb–Pb collisions at $\sqrt{s_{\mathrm{NN}}}$ = 2.76 TeV with ALICE”, *Phys. Rev. C* **88** (2013) 044909, arXiv:1301.4361 [nucl-ex].

[100] X.-N. Wang and M. Gyulassy, “HIJING: A Monte Carlo model for multiple jet production in p p, p A and A A collisions”, *Phys. Rev. D* **44** (1991) 3501–3516.

[101] M. Gyulassy and X.-N. Wang, “HIJING 1.0: A Monte Carlo program for parton and particle production in high-energy hadronic and nuclear collisions”, *Comput. Phys. Commun.* **83** (1994) 307, arXiv:nucl-th/9502021.

[102] R. Brun *et al.*, *GEANT: Detector Description and Simulation Tool*. CERN Program Library. CERN, Geneva, 1993. https://cds.cern.ch/record/1082634. Long Writeup W5013.

[103] R. Barlow, “Systematic errors: Facts and fictions”, in *Conference on Advanced Statistical Techniques in Particle Physics*, pp. 134–144. 7, 2002. arXiv:hep-ex/0207026.

[104] B. Schenke, C. Shen, and P. Tribedy, “Running the gamut of high energy nuclear collisions”, *Phys. Rev. C* **102** (2020) 044905, arXiv:2005.14682 [nucl-th].

[105] H. Mäntysaari, B. Schenke, C. Shen, and W. Zhao, “Bayesian inference of the fluctuating proton shape”, *Phys. Lett. B* **833** (2022) 137348, arXiv:2202.01998 [hep-ph].

[106] Q. Liu, S. Zhao, H.-j. Xu, and H. Song, “Determining the neutron skin thickness by relativistic semi-isobaric collisions”, *Phys. Rev. C* **109** (2024) 034912, arXiv:2311.01747 [nucl-th].

[107] **STAR** Collaboration, M. Abdallah *et al.*, “Collision-System and Beam-Energy Dependence of Anisotropic Flow Fluctuations”, *Phys. Rev. Lett.* **129** (2022) 252301, arXiv:2201.10365 [nucl-ex].

[108] D. Molnar and P. Huovinen, “Dissipative effects from transport and viscous hydrodynamics”, *J. Phys. G* **35** (2008) 104125, arXiv:0806.1367 [nucl-th].

[109] H. Song and U. W. Heinz, “Multiplicity scaling in ideal and viscous hydrodynamics”, *Phys. Rev. C* **78** (2008) 024902, arXiv:0805.1756 [nucl-th].

[110] P. Möller, A. J. Sierk, T. Ichikawa, and H. Sagawa, “Nuclear ground-state masses and deformations: FRDM(2012)”, *Atom. Data Nucl. Data Tabl.* **109-110** (2016) 1–204, arXiv:1508.06294 [nucl-th].

[111] B. H. Alver, C. Gombeaud, M. Luzum, and J.-Y. Ollitrault, “Triangular flow in hydrodynamics and transport theory”, *Phys. Rev. C* **82** (2010) 034913, arXiv:1007.5469 [nucl-th].

[112] **ALICE** Collaboration, S. Acharya *et al.*, “ALICE physics projections for a short oxygen-beam run at the LHC”, ALICE-PUBLIC-2021-004. https://cds.cern.ch/record/2765973.

[113] C. Zhang, J. Chen, G. Giacalone, S. Huang, J. Jia, and Y.-G. Ma, “*Ab-initio* nucleon-nucleon correlations and their impact on high energy ^{16}O+^{16}O collisions”, arXiv:2404.08385 [nucl-th].

[114] Y. Wang, S. Zhao, B. Cao, H.-j. Xu, and H. Song, “Exploring the compactness of α clusters in O16 nuclei with relativistic O16+O16 collisions”, *Phys. Rev. C* **109** (2024) L051904, arXiv:2401.15723 [nucl-th].

[115] B. Bally *et al.*, "Imaging the initial condition of heavy-ion collisions and nuclear structure across the nuclide chart", arXiv:2209.11042 [nucl-ex].

A The ALICE Collaboration

S. Acharya[127], A. Agarwal[135], G. Aglieri Rinella[32], L. Aglietta[24], M. Agnello[29], N. Agrawal[25], Z. Ahammed[135], S. Ahmad[15], S.U. Ahn[71], I. Ahuja[37], A. Akindinov[141], V. Akishina[38], M. Al-Turany[97], D. Aleksandrov[141], B. Alessandro[56], H.M. Alfanda[6], R. Alfaro Molina[67], B. Ali[15], A. Alici[25], N. Alizadehvandchali[116], A. Alkin[104], J. Alme[20], G. Alocco[24,52], T. Alt[64], A.R. Altamura[50], I. Altsybeev[95], J.R. Alvarado[44], C.O.R. Alvarez[44], M.N. Anaam[6], C. Andrei[45], N. Andreou[115], A. Andronic[126], E. Andronov[141], V. Anguelov[94], F. Antinori[54], P. Antonioli[51], N. Apadula[74], L. Aphecetche[103], H. Appelshäuser[64], C. Arata[73], S. Arcelli[25], R. Arnaldi[56], J.G.M.C.A. Arneiro[110], I.C. Arsene[19], M. Arslandok[138], A. Augustinus[32], R. Averbeck[97], D. Averyanov[141], M.D. Azmi[15], H. Baba[124], A. Badalà[53], J. Bae[104], Y.W. Baek[40], X. Bai[120], R. Bailhache[64], Y. Bailung[48], R. Bala[91], A. Balbino[29], A. Baldisseri[130], B. Balis[2], Z. Banoo[91], V. Barbasova[37], F. Barile[31], L. Barioglio[56], M. Barlou[78], B. Barman[41], G.G. Barnaföldi[46], L.S. Barnby[115], E. Barreau[103], V. Barret[127], L. Barreto[110], C. Bartels[119], K. Barth[32], E. Bartsch[64], N. Bastid[127], S. Basu[75], G. Batigne[103], D. Battistini[95], B. Batyunya[142], D. Bauri[47], J.L. Bazo Alba[101], I.G. Bearden[83], C. Beattie[138], P. Becht[97], D. Behera[48], I. Belikov[129], A.D.C. Bell Hechavarria[126], F. Bellini[25], R. Bellwied[116], S. Belokurova[141], L.G.E. Beltran[109], Y.A.V. Beltran[44], G. Bencedi[46], A. Bensaoula[116], S. Beole[24], Y. Berdnikov[141], A. Berdnikova[94], L. Bergmann[94], M.G. Besoiu[63], L. Betev[32], P.P. Bhaduri[135], A. Bhasin[91], B. Bhattacharjee[41], L. Bianchi[24], J. Bielčík[35], J. Bielčíková[86], A.P. Bigot[129], A. Bilandzic[95], G. Biro[46], S. Biswas[4], N. Bize[103], J.T. Blair[108], D. Blau[141], M.B. Blidaru[97], N. Bluhme[38], C. Blume[64], G. Boca[21,55], F. Bock[87], T. Bodova[20], J. Bok[16], L. Boldizsár[46], M. Bombara[37], P.M. Bond[32], G. Bonomi[134,55], H. Borel[130], A. Borissov[141], A.G. Borquez Carcamo[94], E. Botta[24], Y.E.M. Bouziani[64], L. Bratrud[64], P. Braun-Munzinger[97], M. Bregant[110], M. Broz[35], G.E. Bruno[96,31], V.D. Buchakchiev[36], M.D. Buckland[85], D. Budnikov[141], H. Buesching[64], S. Bufalino[29], P. Buhler[102], N. Burmasov[141], Z. Buthelezi[68,123], A. Bylinkin[20], S.A. Bysiak[107], J.C. Cabanillas Noris[109], M.F.T. Cabrera[116], M. Cai[6], H. Caines[138], A. Caliva[28], E. Calvo Villar[101], J.M.M. Camacho[109], P. Camerini[23], F.D.M. Canedo[110], S.L. Cantway[138], M. Carabas[113], A.A. Carballo[32], F. Carnesecchi[32], R. Caron[128], L.A.D. Carvalho[110], J. Castillo Castellanos[130], M. Castoldi[32], F. Catalano[32], S. Cattaruzzi[23], C. Ceballos Sanchez[7], R. Cerri[24], I. Chakaberia[74], P. Chakraborty[136], S. Chandra[135], S. Chapeland[32], M. Chartier[119], S. Chattopadhay[135], S. Chattopadhyay[135], S. Chattopadhyay[99], M. Chen[39], T. Cheng[6], C. Cheshkov[128], V. Chibante Barroso[32], D.D. Chinellato[102], E.S. Chizzali[II,95], J. Cho[58], S. Cho[58], P. Chochula[32], Z.A. Chochulska[136], D. Choudhury[41], P. Christakoglou[84], C.H. Christensen[83], P. Christiansen[75], T. Chujo[125], M. Ciacco[29], C. Cicalo[52], M.R. Ciupek[97], G. Clai[III,51], F. Colamaria[50], J.S. Colburn[100], D. Colella[31], A. Colelli[31], M. Colocci[25], M. Concas[32], G. Conesa Balbastre[73], Z. Conesa del Valle[131], G. Contin[23], J.G. Contreras[35], M.L. Coquet[103], P. Cortese[133,56], M.R. Cosentino[112], F. Costa[32], S. Costanza[21,55], C. Cot[131], P. Crochet[127], R. Cruz-Torres[74], M.M. Czarnynoga[136], A. Dainese[54], G. Dange[38], M.C. Danisch[94], A. Danu[63], P. Das[80], S. Das[4], A.R. Dash[126], S. Dash[47], A. De Caro[28], G. de Cataldo[50], J. de Cuveland[38], A. De Falco[22], D. De Gruttola[28], N. De Marco[56], C. De Martin[23], S. De Pasquale[28], R. Deb[134], R. Del Grande[95], L. Dello Stritto[32], W. Deng[6], K.C. Devereaux[18], P. Dhankher[18], D. Di Bari[31], A. Di Mauro[32], B. Di Ruzza[132], B. Diab[130], R.A. Diaz[142,7], T. Dietel[114], Y. Ding[6], J. Ditzel[64], R. Divià[32], Ø. Djuvsland[20], U. Dmitrieva[141], A. Dobrin[63], B. Dönigus[64], J.M. Dubinski[136], A. Dubla[97], P. Dupieux[127], N. Dzalaiova[13], T.M. Eder[126], R.J. Ehlers[74], F. Eisenhut[64], R. Ejima[92], D. Elia[50], B. Erazmus[103], F. Ercolessi[25], B. Espagnon[131], G. Eulisse[32], D. Evans[100], S. Evdokimov[141], L. Fabbietti[95], M. Faggin[23], J. Faivre[73], F. Fan[6], W. Fan[74], A. Fantoni[49], M. Fasel[87], A. Feliciello[56], G. Feofilov[141], A. Fernández Téllez[44], L. Ferrandi[110], M.B. Ferrer[32], A. Ferrero[130], C. Ferrero[IV,56], A. Ferretti[24], V.J.G. Feuillard[94], V. Filova[35], D. Finogeev[141], F.M. Fionda[52], E. Flatland[32], F. Flor[138,116], A.N. Flores[108], S. Foertsch[68], I. Fokin[94], S. Fokin[141], U. Follo[IV,56], E. Fragiacomo[57], E. Frajna[46], U. Fuchs[32], N. Funicello[28], C. Furget[73], A. Furs[141], T. Fusayasu[98], J.J. Gaardhøje[83], M. Gagliardi[24], A.M. Gago[101], T. Gahlaut[47], C.D. Galvan[109], S. Gami[80], D.R. Gangadharan[116], P. Ganoti[78], C. Garabatos[97], J.M. Garcia[44], T. García Chávez[44], E. Garcia-Solis[9], C. Gargiulo[32], P. Gasik[97], H.M. Gaur[38], A. Gautam[118], M.B. Gay Ducati[66], M. Germain[103], R.A. Gernhaeuser[95], C. Ghosh[135], M. Giacalone[51], G. Gioachin[29], S.K. Giri[135], P. Giubellino[97,56], P. Giubilato[27], A.M.C. Glaenzer[130], P. Glässel[94], E. Glimos[122], D.J.Q. Goh[76], V. Gonzalez[137], P. Gordeev[141], M. Gorgon[2], K. Goswami[48], S. Gotovac[33], V. Grabski[67], L.K. Graczykowski [136], E. Grecka [86], A. Grelli [59], C. Grigoras [32], V. Grigoriev [141], S. Grigoryan [142,1], F. Grosa [32], J.F. Grosse-Oetringhaus [32], R. Grosso [97], D. Grund [35], N.A. Grunwald[94], G.G. Guardiano [111], R. Guernane [73], M. Guilbaud [103], K. Gulbrandsen [83], J.J.W.K. Gumprecht[102], T. Gündem [64], T. Gunji [124], W. Guo [6], A. Gupta [91], R. Gupta [91], R. Gupta [48], K. Gwizdziel [136], L. Gyulai [46], C. Hadjidakis [131], F.U. Haider [91], S. Haidlova [35], M. Haldar[4], H. Hamagaki [76], Y. Han [139], B.G. Hanley [137], R. Hannigan [108], J. Hansen [75], M.R. Haque [97], J.W. Harris [138], A. Harton [9], M.V. Hartung [64], H. Hassan [117], D. Hatzifotiadou [51], P. Hauer [42], L.B. Havener [138], E. Hellbär [32], H. Helstrup [34], M. Hemmer [64], T. Herman [35], S.G. Hernandez[116], G. Herrera Corral [8], S. Herrmann [128], K.F. Hetland [34], B. Heybeck [64], H. Hillemanns [32], B. Hippolyte [129], I.P.M. Hobus[84], F.W. Hoffmann [70], B. Hofman [59], G.H. Hong [139], M. Horst [95], A. Horzyk [2], Y. Hou [6], P. Hristov [32], P. Huhn[64], L.M. Huhta [117], T.J. Humanic [88], A. Hutson [116], D. Hutter [38], M.C. Hwang [18], R. Ilkaev[141], M. Inaba [125], G.M. Innocenti [32], M. Ippolitov [141], A. Isakov [84], T. Isidori [118], M.S. Islam [99], S. Iurchenko[141], M. Ivanov [97], M. Ivanov[13], V. Ivanov [141], K.E. Iversen [75], M. Jablonski [2], B. Jacak [18,74], N. Jacazio [25], P.M. Jacobs [74], S. Jadlovska[106], J. Jadlovsky[106], S. Jaelani [82], C. Jahnke [110], M.J. Jakubowska [136], M.A. Janik [136], T. Janson[70], S. Ji [16], S. Jia [10], T. Jiang [10], A.A.P. Jimenez [65], F. Jonas [74], D.M. Jones [119], J.M. Jowett [32,97], J. Jung [64], M. Jung [64], A. Junique [32], A. Jusko [100], J. Kaewjai[105], P. Kalinak [60], A. Kalweit [32], A. Karasu Uysal [V,72], D. Karatovic [89], N. Karatzenis[100], O. Karavichev [141], T. Karavicheva [141], E. Karpechev [141], M.J. Karwowska [32,136], U. Kebschull [70], R. Keidel [140], M. Keil [32], B. Ketzer [42], J. Keul [64], S.S. Khade [48], A.M. Khan [120], S. Khan [15], A. Khanzadeev [141], Y. Kharlov [141], A. Khatun [118], A. Khuntia [35], Z. Khuranova [64], B. Kileng [34], B. Kim [104], C. Kim [16], D.J. Kim [117], E.J. Kim [69], J. Kim [139], J. Kim [58], J. Kim [32,69], M. Kim [18], S. Kim [17], T. Kim [139], K. Kimura [92], A. Kirkova[36], S. Kirsch [64], I. Kisel [38], S. Kiselev [141], A. Kisiel [136], J.P. Kitowski [2], J.L. Klay [5], J. Klein [32], S. Klein [74], C. Klein-Bösing [126], M. Kleiner [64], T. Klemenz [95], A. Kluge [32], C. Kobdaj [105], R. Kohara[124], T. Kollegger[97], A. Kondratyev [142], N. Kondratyeva [141], J. Konig [64], S.A. Konigstorfer [95], P.J. Konopka [32], G. Kornakov [136], M. Korwieser [95], S.D. Koryciak [2], C. Koster[84], A. Kotliarov [86], N. Kovacic[89], V. Kovalenko [141], M. Kowalski [107], V. Kozhuharov [36], G. Kozlov[38], I. Králik [60], A. Kravčáková [37], L. Krcal [32,38], M. Krivda [100,60], F. Krizek [86], K. Krizkova Gajdosova [32], C. Krug [66], M. Krüger [64], D.M. Krupova [35], E. Kryshen [141], V. Kučera [58], C. Kuhn [129], P.G. Kuijer [84], T. Kumaoka[125], D. Kumar[135], L. Kumar [90], N. Kumar[90], S. Kumar [50], S. Kundu [32], P. Kurashvili [79], A. Kurepin [141], A.B. Kurepin [141], A. Kuryakin [141], S. Kushpil [86], V. Kuskov [141], M. Kutyla[136], A. Kuznetsov[142], M.J. Kweon [58], Y. Kwon [139], S.L. La Pointe [38], P. La Rocca [26], A. Lakrathok[105], M. Lamanna [32], A.R. Landou [73], R. Langoy [121], P. Larionov [32], E. Laudi [32], L. Lautner [32,95], R.A.N. Laveaga[109], R. Lavicka [102], R. Lea [134,55], H. Lee [104], I. Legrand [45], G. Legras [126], J. Lehrbach [38], A.M. Lejeune[35], T.M. Lelek[2], R.C. Lemmon [I,85], I. León Monzón [109], M.M. Lesch [95], E.D. Lesser [18], P. Lévai [46], M. Li[6], P. Li[10], X. Li[10], B.E. Liang-gilman [18], J. Lien [121], R. Lietava [100], I. Likmeta [116], B. Lim [24], S.H. Lim [16], V. Lindenstruth [38], C. Lippmann [97], D.H. Liu [6], J. Liu [119], G.S.S. Liveraro [111], I.M. Lofnes [20], C. Loizides [87], S. Lokos [107], J. Lömker [59], X. Lopez [127], E. López Torres [7], C. Lotteau[128], P. Lu [97,120], Z. Lu [10], F.V. Lugo [67], J.R. Luhder [126], M. Lunardon [27], G. Luparello [57], Y.G. Ma [39], M. Mager [32], A. Maire [129], E.M. Majerz[2], M.V. Makariev [36], M. Malaev [141], G. Malfattore [25], N.M. Malik [91], S.K. Malik [91], L. Malinina [I,VIII,142], D. Mallick [131], N. Mallick [48], G. Mandaglio [30,53], S.K. Mandal [79], A. Manea [63], V. Manko [141], F. Manso [127], V. Manzari [50], Y. Mao [6], R.W. Marcjan [2], G.V. Margagliotti [23], A. Margotti [51], A. Marín [97], C. Markert [108], C.F.B. Marquez[31], P. Martinengo [32], M.I. Martínez [44], G. Martínez García [103], M.P.P. Martins [110], S. Masciocchi [97], M. Masera [24], A. Masoni [52], L. Massacrier [131], O. Massen [59], A. Mastroserio [132,50], O. Matonoha [75], S. Mattiazzo [27], A. Matyja [107], F. Mazzaschi [32,24], M. Mazzilli [116], Y. Melikyan [43], M. Melo [110], A. Menchaca-Rocha [67], J.E.M. Mendez [65], E. Meninno [102], A.S. Menon [116], M.W. Menzel[32,94], M. Meres [13], Y. Miake[125], L. Micheletti [32], D.L. Mihaylov [95], K. Mikhaylov [142,141], N. Minafra [118], D. Miśkowiec [97], A. Modak [134], B. Mohanty[80], M. Mohisin Khan [VI,15], M.A. Molander [43], S. Monira [136], C. Mordasini [117], D.A. Moreira De Godoy [126], I. Morozov [141], A. Morsch [32], T. Mrnjavac [32], V. Muccifora [49], S. Muhuri [135], J.D. Mulligan [74], A. Mulliri [22], M.G. Munhoz [110], R.H. Munzer [64], H. Murakami [124], S. Murray [114], L. Musa [32], J. Musinsky [60], J.W. Myrcha [136], B. Naik [123], A.I. Nambrath [18], B.K. Nandi [47], R. Nania [51], E. Nappi [50], A.F. Nassirpour [17], A. Nath [94], S. Nath[135], C. Nattrass [122], M.N. Naydenov [36], A. Neagu[19], A. Negru[113], E. Nekrasova[141], L. Nellen [65], R. Nepeivoda [75], S. Nese [19], N. Nicassio [50], B.S. Nielsen [83], E.G. Nielsen [83], S. Nikolaev [141], S. Nikulin [141], V. Nikulin [141], F. Noferini [51], S. Noh [12], P. Nomokonov [142],

J. Norman [119], N. Novitzky [87], P. Nowakowski [136], A. Nyanin [141], J. Nystrand [20], S. Oh [17],
A. Ohlson [75], V.A. Okorokov [141], J. Oleniacz [136], A. Onnerstad [117], C. Oppedisano [56], A. Ortiz
Velasquez [65], J. Otwinowski [107], M. Oya[92], K. Oyama [76], Y. Pachmayer [94], S. Padhan [47],
D. Pagano [134,55], G. Paić [65], S. Paisano-Guzmán [44], A. Palasciano [50], I. Panasenko[75], S. Panebianco [130],
C. Pantouvakis [27], H. Park [125], H. Park [104], J. Park [125], J.E. Parkkila [32], Y. Patley [47], R.N. Patra[50],
B. Paul [135], H. Pei [6], T. Peitzmann [59], X. Peng [11], M. Pennisi [24], S. Perciballi [24], D. Peresunko [141],
G.M. Perez [7], Y. Pestov[141], M.T. Petersen[83], V. Petrov [141], M. Petrovici [45], S. Piano [57], M. Pikna [13],
P. Pillot [103], O. Pinazza [51,32], L. Pinsky[116], C. Pinto [95], S. Pisano [49], M. Płoskoń [74], M. Planinic[89],
F. Pliquett[64], D.K. Plociennik [2], M.G. Poghosyan [87], B. Polichtchouk [141], S. Politano [29], N. Poljak [89],
A. Pop [45], S. Porteboeuf-Houssais [127], V. Pozdniakov [I,142], I.Y. Pozos [44], K.K. Pradhan [48],
S.K. Prasad [4], S. Prasad [48], R. Preghenella [51], F. Prino [56], C.A. Pruneau [137], I. Pshenichnov [141],
M. Puccio [32], S. Pucillo [24], S. Qiu [84], L. Quaglia [24], A.M.K. Radhakrishnan[48], S. Ragoni [14],
A. Rai [138], A. Rakotozafindrabe [130], L. Ramello [133,56], F. Rami [129], M. Rasa [26], S.S. Räsänen [43],
R. Rath [51], M.P. Rauch [20], I. Ravasenga [32], K.F. Read [87,122], C. Reckziegel [112], A.R. Redelbach [38],
K. Redlich [VII,79], C.A. Reetz [97], H.D. Regules-Medel[44], A. Rehman[20], F. Reidt [32], H.A. Reme-Ness [34],
K. Reygers [94], A. Riabov [141], V. Riabov [141], R. Ricci [28], M. Richter [20], A.A. Riedel [95],
W. Riegler [32], A.G. Riffero [24], M. Rignanese [27], C. Ripoli[28], C. Ristea [63], M.V. Rodriguez [32],
M. Rodríguez Cahuantzi [44], S.A. Rodríguez Ramírez [44], K. Røed [19], R. Rogalev [141], E. Rogochaya [142],
T.S. Rogoschinski [64], D. Rohr [32], D. Röhrich [20], S. Rojas Torres [35], P.S. Rokita [136], G. Romanenko [25],
F. Ronchetti [32], E.D. Rosas[65], K. Roslon [136], A. Rossi [54], A. Roy [48], S. Roy [47], N. Rubini [51,25],
J.A. Rudolph[84], D. Ruggiano [136], R. Rui [23], P.G. Russek [2], R. Russo [84], A. Rustamov [81],
E. Ryabinkin [141], Y. Ryabov [141], A. Rybicki [107], J. Ryu [16], W. Rzesa [136], B. Sabiu[51], S. Sadovsky [141],
J. Saetre [20], K. Šafařík [35], S. Saha [80], B. Sahoo [48], R. Sahoo [48], S. Sahoo[61], D. Sahu [48], P.K. Sahu [61],
J. Saini [135], K. Sajdakova[37], S. Sakai [125], M.P. Salvan [97], S. Sambyal [91], D. Samitz [102], I. Sanna [32,95],
T.B. Saramela[110], D. Sarkar [83], P. Sarma [41], V. Sarritzu [22], V.M. Sarti [95], M.H.P. Sas [32], S. Sawan [80],
E. Scapparone [51], J. Schambach [87], H.S. Scheid [64], C. Schiaua [45], R. Schicker [94], F. Schlepper [94],
A. Schmah[97], C. Schmidt [97], H.R. Schmidt[93], M.O. Schmidt [32], M. Schmidt[93], N.V. Schmidt [87],
A.R. Schmier [122], R. Schotter [102,129], A. Schröter [38], J. Schukraft [32], K. Schweda [97], G. Scioli [25],
E. Scomparin [56], J.E. Seger [14], Y. Sekiguchi[124], D. Sekihata [124], M. Selina [84], I. Selyuzhenkov [97],
S. Senyukov [129], J.J. Seo [94], D. Serebryakov [141], L. Serkin [65], L. Šerkšnytė [95], A. Sevcenco [63],
T.J. Shaba [68], A. Shabetai [103], R. Shahoyan[32], A. Shangaraev [141], B. Sharma [91], D. Sharma [47],
H. Sharma [54], M. Sharma [91], S. Sharma [76], S. Sharma [91], U. Sharma [91], A. Shatat [131], O. Sheibani[116],
K. Shigaki [92], M. Shimomura[77], J. Shin[12], S. Shirinkin [141], Q. Shou [39], Y. Sibiriak [141], S. Siddhanta [52],
T. Siemiarczuk [79], T.F. Silva [110], D. Silvermyr [75], T. Simantathammakul[105], R. Simeonov [36], B. Singh[91],
B. Singh [95], K. Singh [48], R. Singh [80], R. Singh [91], R. Singh [97], S. Singh [15], V.K. Singh [135],
V. Singhal [135], T. Sinha [99], B. Sitar [13], M. Sitta [133,56], T.B. Skaali[19], G. Skorodumovs [94],
N. Smirnov [138], R.J.M. Snellings [59], E.H. Solheim [19], J. Song [16], C. Sonnabend [32,97],
J.M. Sonneveld [84], F. Soramel [27], A.B. Soto-hernandez [88], R. Spijkers [84], I. Sputowska [107], J. Staa [75],
J. Stachel [94], I. Stan [63], P.J. Steffanic [122], T. Stellhorn[126], S.F. Stiefelmaier [94], D. Stocco [103],
I. Storehaug [19], N.J. Strangmann [64], P. Stratmann [126], S. Strazzi [25], A. Sturniolo [30,53], C.P. Stylianidis[84],
A.A.P. Suaide [110], C. Suire [131], M. Sukhanov [141], M. Suljic [32], R. Sultanov [141], V. Sumberia [91],
S. Sumowidagdo [82], M. Szymkowski [136], S.F. Taghavi [95], G. Taillepied [97], J. Takahashi [111],
G.J. Tambave [80], S. Tang [6], Z. Tang [120], J.D. Tapia Takaki [118], N. Tapus[113], L.A. Tarasovicova [37],
M.G. Tarzila [45], G.F. Tassielli [31], A. Tauro [32], A. Tavira García [131], G. Tejeda Muñoz [44], L. Terlizzi [24],
C. Terrevoli [50], S. Thakur [4], D. Thomas [108], A. Tikhonov [141], N. Tiltmann [32,126], A.R. Timmins [116],
M. Tkacik[106], T. Tkacik [106], A. Toia [64], R. Tokumoto[92], S. Tomassini[25], K. Tomohiro[92], N. Topilskaya [141],
M. Toppi [49], V.V. Torres [103], A.G. Torres Ramos [31], A. Trifiró [30,53], T. Triloki[96], A.S. Triolo [32,30,53],
S. Tripathy [32], T. Tripathy [47], S. Trogolo [24], V. Trubnikov [3], W.H. Trzaska [117], T.P. Trzcinski [136],
C. Tsolanta[19], R. Tu[39], A. Tumkin [141], R. Turrisi [54], T.S. Tveter [19], K. Ullaland [20], B. Ulukutlu [95],
S. Upadhyaya [107], A. Uras [128], M. Urioni [134], G.L. Usai [22], M. Vala[37], N. Valle [55], L.V.R. van
Doremalen[59], M. van Leeuwen [84], C.A. van Veen [94], R.J.G. van Weelden [84], P. Vande Vyvre [32],
D. Varga [46], Z. Varga [46], P. Vargas Torres[65], M. Vasileiou [78], A. Vasiliev [I,141], O. Vázquez Doce [49],
O. Vazquez Rueda [116], V. Vechernin [141], E. Vercellin [24], S. Vergara Limón[44], R. Verma [47],
L. Vermunt [97], R. Vértesi [46], M. Verweij [59], L. Vickovic[33], Z. Vilakazi[123], O. Villalobos Baillie [100],
A. Villani [23], A. Vinogradov [141], T. Virgili [28], M.M.O. Virta [117], A. Vodopyanov [142], B. Volkel [32],
M.A. Völkl [94], S.A. Voloshin [137], G. Volpe [31], B. von Haller [32], I. Vorobyev [32], N. Vozniuk [141],

J. Vrláková [37], J. Wan[39], C. Wang [39], D. Wang[39], Y. Wang [39], Y. Wang [6], Z. Wang [39], A. Wegrzynek [32], F.T. Weiglhofer[38], S.C. Wenzel [32], J.P. Wessels [126], J. Wiechula [64], J. Wikne [19], G. Wilk [79], J. Wilkinson [97], G.A. Willems [126], B. Windelband [94], M. Winn [130], J.R. Wright [108], W. Wu[39], Y. Wu [120], Z. Xiong[120], R. Xu [6], A. Yadav [42], A.K. Yadav [135], Y. Yamaguchi [92], S. Yang[20], S. Yano [92], E.R. Yeats[18], Z. Yin [6], I.-K. Yoo [16], J.H. Yoon [58], H. Yu[12], S. Yuan[20], A. Yuncu [94], V. Zaccolo [23], C. Zampolli [32], F. Zanone [94], N. Zardoshti [32], A. Zarochentsev [141], P. Závada [62], N. Zaviyalov[141], M. Zhalov [141], B. Zhang [94,6], C. Zhang [130], L. Zhang [39], M. Zhang [127,6], M. Zhang [6], S. Zhang [39], X. Zhang [6], Y. Zhang[120], Z. Zhang [6], M. Zhao [10], V. Zherebchevskii [141], Y. Zhi[10], D. Zhou [6], Y. Zhou [83], J. Zhu [54,6], S. Zhu[120], Y. Zhu[6], S.C. Zugravel [56], N. Zurlo [134,55]

Affiliation Notes

[I] Deceased
[II] Also at: Max-Planck-Institut fur Physik, Munich, Germany
[III] Also at: Italian National Agency for New Technologies, Energy and Sustainable Economic Development (ENEA), Bologna, Italy
[IV] Also at: Dipartimento DET del Politecnico di Torino, Turin, Italy
[V] Also at: Yildiz Technical University, Istanbul, Türkiye
[VI] Also at: Department of Applied Physics, Aligarh Muslim University, Aligarh, India
[VII] Also at: Institute of Theoretical Physics, University of Wroclaw, Poland
[VIII] Also at: An institution covered by a cooperation agreement with CERN

Collaboration Institutes

[1] A.I. Alikhanyan National Science Laboratory (Yerevan Physics Institute) Foundation, Yerevan, Armenia
[2] AGH University of Krakow, Cracow, Poland
[3] Bogolyubov Institute for Theoretical Physics, National Academy of Sciences of Ukraine, Kiev, Ukraine
[4] Bose Institute, Department of Physics and Centre for Astroparticle Physics and Space Science (CAPSS), Kolkata, India
[5] California Polytechnic State University, San Luis Obispo, California, United States
[6] Central China Normal University, Wuhan, China
[7] Centro de Aplicaciones Tecnológicas y Desarrollo Nuclear (CEADEN), Havana, Cuba
[8] Centro de Investigación y de Estudios Avanzados (CINVESTAV), Mexico City and Mérida, Mexico
[9] Chicago State University, Chicago, Illinois, United States
[10] China Institute of Atomic Energy, Beijing, China
[11] China University of Geosciences, Wuhan, China
[12] Chungbuk National University, Cheongju, Republic of Korea
[13] Comenius University Bratislava, Faculty of Mathematics, Physics and Informatics, Bratislava, Slovak Republic
[14] Creighton University, Omaha, Nebraska, United States
[15] Department of Physics, Aligarh Muslim University, Aligarh, India
[16] Department of Physics, Pusan National University, Pusan, Republic of Korea
[17] Department of Physics, Sejong University, Seoul, Republic of Korea
[18] Department of Physics, University of California, Berkeley, California, United States
[19] Department of Physics, University of Oslo, Oslo, Norway
[20] Department of Physics and Technology, University of Bergen, Bergen, Norway
[21] Dipartimento di Fisica, Università di Pavia, Pavia, Italy
[22] Dipartimento di Fisica dell'Università and Sezione INFN, Cagliari, Italy
[23] Dipartimento di Fisica dell'Università and Sezione INFN, Trieste, Italy
[24] Dipartimento di Fisica dell'Università and Sezione INFN, Turin, Italy
[25] Dipartimento di Fisica e Astronomia dell'Università and Sezione INFN, Bologna, Italy
[26] Dipartimento di Fisica e Astronomia dell'Università and Sezione INFN, Catania, Italy
[27] Dipartimento di Fisica e Astronomia dell'Università and Sezione INFN, Padova, Italy
[28] Dipartimento di Fisica 'E.R. Caianiello' dell'Università and Gruppo Collegato INFN, Salerno, Italy
[29] Dipartimento DISAT del Politecnico and Sezione INFN, Turin, Italy
[30] Dipartimento di Scienze MIFT, Università di Messina, Messina, Italy
[31] Dipartimento Interateneo di Fisica 'M. Merlin' and Sezione INFN, Bari, Italy

[32] European Organization for Nuclear Research (CERN), Geneva, Switzerland
[33] Faculty of Electrical Engineering, Mechanical Engineering and Naval Architecture, University of Split, Split, Croatia
[34] Faculty of Engineering and Science, Western Norway University of Applied Sciences, Bergen, Norway
[35] Faculty of Nuclear Sciences and Physical Engineering, Czech Technical University in Prague, Prague, Czech Republic
[36] Faculty of Physics, Sofia University, Sofia, Bulgaria
[37] Faculty of Science, P.J. Šafárik University, Košice, Slovak Republic
[38] Frankfurt Institute for Advanced Studies, Johann Wolfgang Goethe-Universität Frankfurt, Frankfurt, Germany
[39] Fudan University, Shanghai, China
[40] Gangneung-Wonju National University, Gangneung, Republic of Korea
[41] Gauhati University, Department of Physics, Guwahati, India
[42] Helmholtz-Institut für Strahlen- und Kernphysik, Rheinische Friedrich-Wilhelms-Universität Bonn, Bonn, Germany
[43] Helsinki Institute of Physics (HIP), Helsinki, Finland
[44] High Energy Physics Group, Universidad Autónoma de Puebla, Puebla, Mexico
[45] Horia Hulubei National Institute of Physics and Nuclear Engineering, Bucharest, Romania
[46] HUN-REN Wigner Research Centre for Physics, Budapest, Hungary
[47] Indian Institute of Technology Bombay (IIT), Mumbai, India
[48] Indian Institute of Technology Indore, Indore, India
[49] INFN, Laboratori Nazionali di Frascati, Frascati, Italy
[50] INFN, Sezione di Bari, Bari, Italy
[51] INFN, Sezione di Bologna, Bologna, Italy
[52] INFN, Sezione di Cagliari, Cagliari, Italy
[53] INFN, Sezione di Catania, Catania, Italy
[54] INFN, Sezione di Padova, Padova, Italy
[55] INFN, Sezione di Pavia, Pavia, Italy
[56] INFN, Sezione di Torino, Turin, Italy
[57] INFN, Sezione di Trieste, Trieste, Italy
[58] Inha University, Incheon, Republic of Korea
[59] Institute for Gravitational and Subatomic Physics (GRASP), Utrecht University/Nikhef, Utrecht, Netherlands
[60] Institute of Experimental Physics, Slovak Academy of Sciences, Košice, Slovak Republic
[61] Institute of Physics, Homi Bhabha National Institute, Bhubaneswar, India
[62] Institute of Physics of the Czech Academy of Sciences, Prague, Czech Republic
[63] Institute of Space Science (ISS), Bucharest, Romania
[64] Institut für Kernphysik, Johann Wolfgang Goethe-Universität Frankfurt, Frankfurt, Germany
[65] Instituto de Ciencias Nucleares, Universidad Nacional Autónoma de México, Mexico City, Mexico
[66] Instituto de Física, Universidade Federal do Rio Grande do Sul (UFRGS), Porto Alegre, Brazil
[67] Instituto de Física, Universidad Nacional Autónoma de México, Mexico City, Mexico
[68] iThemba LABS, National Research Foundation, Somerset West, South Africa
[69] Jeonbuk National University, Jeonju, Republic of Korea
[70] Johann-Wolfgang-Goethe Universität Frankfurt Institut für Informatik, Fachbereich Informatik und Mathematik, Frankfurt, Germany
[71] Korea Institute of Science and Technology Information, Daejeon, Republic of Korea
[72] KTO Karatay University, Konya, Turkey
[73] Laboratoire de Physique Subatomique et de Cosmologie, Université Grenoble-Alpes, CNRS-IN2P3, Grenoble, France
[74] Lawrence Berkeley National Laboratory, Berkeley, California, United States
[75] Lund University Department of Physics, Division of Particle Physics, Lund, Sweden
[76] Nagasaki Institute of Applied Science, Nagasaki, Japan
[77] Nara Women's University (NWU), Nara, Japan
[78] National and Kapodistrian University of Athens, School of Science, Department of Physics , Athens, Greece
[79] National Centre for Nuclear Research, Warsaw, Poland
[80] National Institute of Science Education and Research, Homi Bhabha National Institute, Jatni, India
[81] National Nuclear Research Center, Baku, Azerbaijan
[82] National Research and Innovation Agency - BRIN, Jakarta, Indonesia

[83] Niels Bohr Institute, University of Copenhagen, Copenhagen, Denmark
[84] Nikhef, National institute for subatomic physics, Amsterdam, Netherlands
[85] Nuclear Physics Group, STFC Daresbury Laboratory, Daresbury, United Kingdom
[86] Nuclear Physics Institute of the Czech Academy of Sciences, Husinec-Řež, Czech Republic
[87] Oak Ridge National Laboratory, Oak Ridge, Tennessee, United States
[88] Ohio State University, Columbus, Ohio, United States
[89] Physics department, Faculty of science, University of Zagreb, Zagreb, Croatia
[90] Physics Department, Panjab University, Chandigarh, India
[91] Physics Department, University of Jammu, Jammu, India
[92] Physics Program and International Institute for Sustainability with Knotted Chiral Meta Matter (SKCM2), Hiroshima University, Hiroshima, Japan
[93] Physikalisches Institut, Eberhard-Karls-Universität Tübingen, Tübingen, Germany
[94] Physikalisches Institut, Ruprecht-Karls-Universität Heidelberg, Heidelberg, Germany
[95] Physik Department, Technische Universität München, Munich, Germany
[96] Politecnico di Bari and Sezione INFN, Bari, Italy
[97] Research Division and ExtreMe Matter Institute EMMI, GSI Helmholtzzentrum für Schwerionenforschung GmbH, Darmstadt, Germany
[98] Saga University, Saga, Japan
[99] Saha Institute of Nuclear Physics, Homi Bhabha National Institute, Kolkata, India
[100] School of Physics and Astronomy, University of Birmingham, Birmingham, United Kingdom
[101] Sección Física, Departamento de Ciencias, Pontificia Universidad Católica del Perú, Lima, Peru
[102] Stefan Meyer Institut für Subatomare Physik (SMI), Vienna, Austria
[103] SUBATECH, IMT Atlantique, Nantes Université, CNRS-IN2P3, Nantes, France
[104] Sungkyunkwan University, Suwon City, Republic of Korea
[105] Suranaree University of Technology, Nakhon Ratchasima, Thailand
[106] Technical University of Košice, Košice, Slovak Republic
[107] The Henryk Niewodniczanski Institute of Nuclear Physics, Polish Academy of Sciences, Cracow, Poland
[108] The University of Texas at Austin, Austin, Texas, United States
[109] Universidad Autónoma de Sinaloa, Culiacán, Mexico
[110] Universidade de São Paulo (USP), São Paulo, Brazil
[111] Universidade Estadual de Campinas (UNICAMP), Campinas, Brazil
[112] Universidade Federal do ABC, Santo Andre, Brazil
[113] Universitatea Nationala de Stiinta si Tehnologie Politehnica Bucuresti, Bucharest, Romania
[114] University of Cape Town, Cape Town, South Africa
[115] University of Derby, Derby, United Kingdom
[116] University of Houston, Houston, Texas, United States
[117] University of Jyväskylä, Jyväskylä, Finland
[118] University of Kansas, Lawrence, Kansas, United States
[119] University of Liverpool, Liverpool, United Kingdom
[120] University of Science and Technology of China, Hefei, China
[121] University of South-Eastern Norway, Kongsberg, Norway
[122] University of Tennessee, Knoxville, Tennessee, United States
[123] University of the Witwatersrand, Johannesburg, South Africa
[124] University of Tokyo, Tokyo, Japan
[125] University of Tsukuba, Tsukuba, Japan
[126] Universität Münster, Institut für Kernphysik, Münster, Germany
[127] Université Clermont Auvergne, CNRS/IN2P3, LPC, Clermont-Ferrand, France
[128] Université de Lyon, CNRS/IN2P3, Institut de Physique des 2 Infinis de Lyon, Lyon, France
[129] Université de Strasbourg, CNRS, IPHC UMR 7178, F-67000 Strasbourg, France, Strasbourg, France
[130] Université Paris-Saclay, Centre d'Etudes de Saclay (CEA), IRFU, Départment de Physique Nucléaire (DPhN), Saclay, France
[131] Université Paris-Saclay, CNRS/IN2P3, IJCLab, Orsay, France
[132] Università degli Studi di Foggia, Foggia, Italy
[133] Università del Piemonte Orientale, Vercelli, Italy
[134] Università di Brescia, Brescia, Italy
[135] Variable Energy Cyclotron Centre, Homi Bhabha National Institute, Kolkata, India

[136] Warsaw University of Technology, Warsaw, Poland
[137] Wayne State University, Detroit, Michigan, United States
[138] Yale University, New Haven, Connecticut, United States
[139] Yonsei University, Seoul, Republic of Korea
[140] Zentrum für Technologie und Transfer (ZTT), Worms, Germany
[141] Affiliated with an institute covered by a cooperation agreement with CERN
[142] Affiliated with an international laboratory covered by a cooperation agreement with CERN.